Optimal Design of Bistable Nonlinear Energy Sink Based on Global Vibration Control

Guo-Xu Wang
Shanghai University
Hu Ding (dinghu3@shu.edu.cn)
Shanghai University https://orcid.org/0000-0003-4301-1108
Li-Qun Chen
Shanghai University

Research Article

Keywords: Vibration control, linear vibration absorber, nonlinear energy sink, differential evolutionary algorithm, multi-objective design

Posted Date: May 24th, 2021

DOI: https://doi.org/10.21203/rs.3.rs-488534/v1

Optimal design of bistable nonlinear energy sink based on global vibration control

Guo-Xu Wang, Hu Ding * and Li-Qun Chen

Shanghai Key Laboratory of Mechanics in Energy Engineering, Shanghai Institute of Applied Mathematics and Mechanics, School of Mechanics and Engineering Science, Shanghai University, Shanghai, 200072, China

Abstract: Although a linear vibration absorber (LVA) or nonlinear energy sink (NES) can effectively mitigate the vibration of the main system in harmonic excitation, the amplitude of the absorber can be very large. Using the single-objective differential evolutionary (DE) algorithm, this paper pioneers the global control of the main system and a bistable NES to achieve decent vibration mitigation effects and decrease the global response of the system. Using the multi-objective DE algorithms and comparing the optimization results of the LVA, this paper proposes multi-objective and multi-parameter design criteria of a bistable NES. The mass ratio, the displacement amplitude, and the mechanical energy are optimization goals. The results show that the maximum amplitude of the main system and the absorber can be controlled at the same level, and the global control strategy does not change the resonance frequency of the main system. Compared with the LVA, the bistable NES has similar vibration mitigation effects with the variation of the mass ratio in the multi-objective optimization. However, the bistable NES can achieve better control over a larger spring stiffness range. Therefore, through single- and multi-objective optimization design, this paper proves the superiority of the bistable NES in the vibration mitigation. Meanwhile, this paper provides an optimization design method for global vibration control.

Keywords: Vibration control; linear vibration absorber; nonlinear energy sink; differential evolutionary algorithm; multi-objective design

* Corresponding author: dinghu3@shu.edu.cn (H. Ding)

1 Introduction

Vibration widely exists in mechanical systems and brings many hazards, so vibration mitigation has always been a hot issue for researchers and engineers. Applying vibration absorbers is an effective means of vibration mitigation. Traditional vibration absorbers, namely tuned mass dampers or linear vibration absorbers (LVAs), are widely used in the vibration mitigation of various systems, like multistory buildings [1], rectangular plates [2], and airfoil models [3]. The LVA is a simple mass-damping-spring structure, but it can only mitigate vibration in a narrow frequency band and may generate new resonance peaks. To cover these shortages of the LVA, Vakakis and Gendelman added strongly nonlinear stiffness into the absorber and realized 1:1 transient resonance at any frequency and irreversible targeted energy transfer from the main system to the absorber in the impulse excitation [4]; Chen et al. realized the multimode vibration mitigation and did not change the resonance frequencies of the composite plate by using the absorber with zero linear stiffness and cubic nonlinear stiffness in the harmonic excitation [5]. This kind of absorber with strong nonlinearity is called a nonlinear energy sink (NES). At present, the NES has been used in the mitigation of relaxation oscillation of moving belt systems [6], shock vibration of fluid-conveying pipes [7], transverse vibration of flexible bladed rotor systems [8], and stochastic vibration of two-story shear buildings [9].

Since the LVA and the NES have better energy robustness and frequency robustness in vibration mitigation respectively, researchers designed adjustable or hybrid absorber structures to realize both these two kinds of robustness. Habib and Kerschen used the equal-peak method to derive a tuning rule of a nonlinear vibration absorber (NVA) and show better performance than the LVA in harmonic excitation [10]. Habib and Romeo designed a tuned bistable NES with characteristics of the LVA in small amplitude and used this absorber to mitigate the vibration of impulsively excited linear systems in a broad energy range [11]. Benacchio designed a magnetic vibration absorber that can realize the NVA with positive linear stiffness, the monostable NES with zero linear stiffness, or the bistable NES with negative linear stiffness [12]. To broaden the initial energy range of effective vibration mitigation, Farid and Genderman chose proper parameter values to let a pendulum absorber or a hybrid vibro-impact NES act as the LVA in small energies and the rotational NES or the vibro-impact NES in large energies [13, 14]. Taghipour et al. combined the LVA and the monostable NES to raise the vibration mitigation efficiency and broaden the stability

range of a nonlinear rotor system [15]. Wang et al. also combined the LVA, the monostable NES, and impact surfaces to enhance both energy robustness and frequency robustness of the absorber in seismic response mitigation [16]. The above studies mainly focused on the improvement in the vibration mitigation effect of the absorbers. However, the absorbers with decent vibration mitigation effects may have large amplitudes, which will shorten their service life [16–18]. At present, the amplitude control of the absorbers is realized by adding protective devices, e.g. impact surfaces [18–20] or piecewise spring devices [21]. This paper will present a new control strategy, i.e. using the optimization algorithm to mitigate both the amplitudes of the main system and the absorber.

In the design of the NES, multiple vibration mitigation measures need considering, such as the amplitude of the main system, energy dissipation rate of the NES, energy decaying duration of the whole system, and transmissibility of the system [22–28]. Besides, other indexes, like the stability range of the response [29] and the economic factors of the structure [30], should be in consideration. In addition, multiple parameters need to be optimized in different NES structures, e.g. the mass ratio and clearance of the vibro-impact NES [20, 31, 32] and the mass ratio, damping, spring stiffness, geometry parameter, and location of the bistable NES [7, 33]. In the multi-objective and multi-parameter optimization of the NES, intelligent optimization algorithms can be used to describe the Pareto front (distribution of non-dominated solutions in the target space). For example, Raj and Santhosh combined a weighting approach and the genetic algorithm to demonstrate the Pareto front of displacement amplitude and voltage response of a harmonically excited nonlinear oscillator coupled with an NVA and an energy harvester [34]. Khazaee used the non-dominated sorting genetic algorithm to display the Pareto front of the expectation and variance of the energy dissipation rate of the NES with parameter uncertainties [7, 35]. In fact, the intelligent optimization algorithm can not only show the characteristics of non-dominated solutions in the target space but show the characteristics of tuning parameters. The latter will help to guide the design of the NES. However, there is little research on the extraction of the design criteria of the NES through the multi-objective intelligent optimization algorithm. On the other hand, the multi-objective design of the NES can refer to that of the LVA. For example, in Wang's study, the optimized single-sided vibro-impact track NES requires smaller damping versus the LVA [30]. In the authors' previous study, the multi-objective optimization results of the LVA and the bistable NES show high

similarity in the impulsive excitation [17]. What about the similarities and disparities of the multi-objective optimization results of the LVA and the bistable NES in the harmonic excitation? This paper will answer this question and propose new multi-objective and multi-parameter design criteria of the bistable NES.

According to the above discussion, this paper is structured as follows. Section 2 describes the models of a linear main system couple with an LVA or an NES. Sections 3 and 4 firstly propose the single-objective optimization issues on the amplitude control of the main system or the whole system in single- or sweep-frequency excitation conditions and then solve these issues by the differential evolutionary (DE) algorithm and the parameter sensitivity analysis. And the characteristics of the frequency responses of the optimal situations are analyzed. In Sections 5 and 6, the multi-objective optimization issues are proposed, and these issues are solved by the multi-objective DE algorithm. The characteristics of the Pareto fronts and the optimized parameters of the LVA and the NES are illustrated. Finally, Section 7 addresses the conclusions.

2 Mechanical model

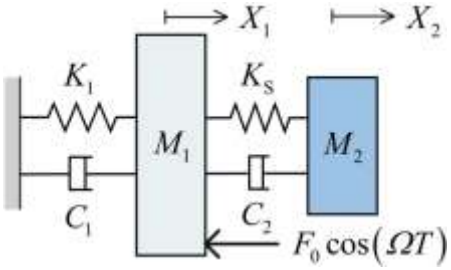

Fig. 1. Model of an LO coupled with an LVA.

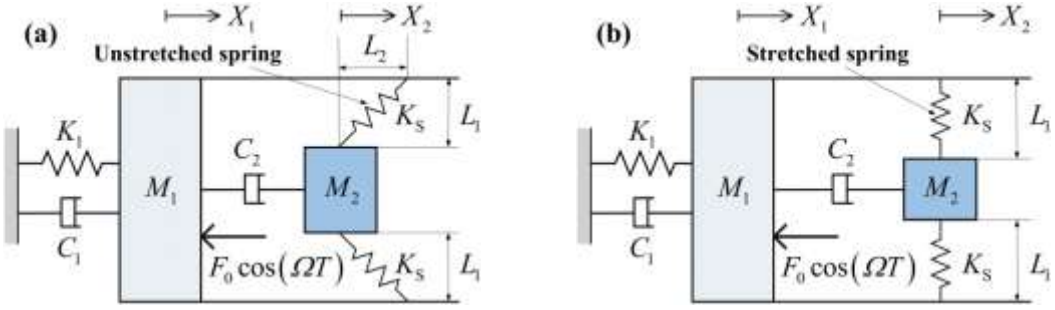

Fig. 2. Model of an LO coupled with an NES: (a) $L_1 \le L$, $L_2 \ge 0$, $L_1^2+L_2^2=L^2$; (b) $L_1 > L$, $L_2=0$.

Fig. 1 and Fig. 2 present the model of a linear oscillator (LO) coupled with an LVA or a classical double-string NES structure [36, 37]. M_1, C_1, and K_1 are the mass, damping, and spring stiffness of the LO. M_2, C_2, and K_S are the mass, damping, and spring stiffness of the two absorbers.

L is the free length of the springs of the absorbers. L_1 and L_2 are the characteristic lengths of the springs of the NES in two directions. By adjusting the distance of the two fixes ends ($2L_1$), the two symmetric springs of the NES can be unstretched or stretched. X_1 and X_2 are the displacements of the LO and the absorber, respectively. F_0 and Ω are the amplitude and frequency of external harmonic force, respectively. By utilizing Newton's law, the dynamic equations of the LO-LVA and the LO-NES systems can be derived as

$$\begin{aligned} &M_1\frac{\mathrm{d}^2X_1}{\mathrm{d}T^2}+C_1\frac{\mathrm{d}X_1}{\mathrm{d}T}+K_1X_1+C_2\left(\frac{\mathrm{d}X_1}{\mathrm{d}T}-\frac{\mathrm{d}X_2}{\mathrm{d}T}\right)+K_\mathrm{S}\left(X_1-X_2\right)+F_0\cos\left(\Omega T\right)=0,\\ &M_2\frac{\mathrm{d}^2X_2}{\mathrm{d}T^2}+C_2\left(\frac{\mathrm{d}X_2}{\mathrm{d}T}-\frac{\mathrm{d}X_1}{\mathrm{d}T}\right)-K_\mathrm{S}\left(X_1-X_2\right)=0. \end{aligned} \tag{1}$$

$$\begin{aligned} &M_1\frac{\mathrm{d}^2X_1}{\mathrm{d}T^2}+C_1\frac{\mathrm{d}X_1}{\mathrm{d}T}+K_1X_1+C_2\left(\frac{\mathrm{d}X_1}{\mathrm{d}T}-\frac{\mathrm{d}X_2}{\mathrm{d}T}\right)+2K_\mathrm{S}\left(X_1-X_2+L_2\right)\left[1-\sqrt{\frac{L_1^2+L_2{}^2}{L_1^2+\left(X_1-X_2+L_2\right)^2}}\right]+F_0\cos\left(\Omega T\right)=0,\\ &M_2\frac{\mathrm{d}^2X_2}{\mathrm{d}T^2}+C_2\left(\frac{\mathrm{d}X_2}{\mathrm{d}T}-\frac{\mathrm{d}X_1}{\mathrm{d}T}\right)-2K_\mathrm{S}\left(X_1-X_2+L_2\right)\left[1-\sqrt{\frac{L_1^2+L_2{}^2}{L_1^2+\left(X_1-X_2+L_2\right)^2}}\right]=0. \end{aligned} \tag{2}$$

The dimensionless forms of Eqs. (1) and (2) are

$$\begin{aligned} &\ddot{x}_1+c_1\dot{x}_1+x_1+c_2\left(\dot{x}_1-\dot{x}_2\right)+k_\mathrm{s}\left(x_1-x_2\right)+f_0\cos\left(\omega t\right)=0,\\ &\varepsilon\ddot{x}_2+c_2\left(\dot{x}_2-\dot{x}_1\right)-k_\mathrm{s}\left(x_1-x_2\right)=0. \end{aligned} \tag{3}$$

$$\begin{aligned} &\ddot{x}_1+c_1\dot{x}_1+x_1+c_2\left(\dot{x}_1-\dot{x}_2\right)+2k_\mathrm{s}\left(x_1-x_2+l_2\right)\left[1-\frac{1}{\sqrt{l_1^2+\left(x_1-x_2+l_2\right)^2}}\right]+f_0\cos\left(\omega t\right)=0,\\ &\varepsilon\ddot{x}_2+c_2\left(\dot{x}_2-\dot{x}_1\right)-2k_\mathrm{s}\left(x_1-x_2+l_2\right)\left[1-\frac{1}{\sqrt{l_1^2+\left(x_1-x_2+l_2\right)^2}}\right]=0. \end{aligned} \tag{4}$$

where the dot (•) is the derivative compared to t. The expressions of dimensionless variables and parameters are

$$\begin{aligned} &\omega_0=\sqrt{\frac{K_1}{M_1}},t=\omega_0T,x_1=\frac{X_1}{L},x_2=\frac{X_2}{L},l_1=\frac{L_1}{L},l_2=\frac{L_2}{L},c_1=\frac{C_1}{M_1\omega_0},\\ &c_2=\frac{C_2}{M_1\omega_0},k_\mathrm{s}=\frac{K_\mathrm{S}}{M_1\omega_0^2},\varepsilon=\frac{M_2}{M_1},f_0=\frac{F_0}{M_1L\omega_0^2},\omega=\frac{\Omega}{\omega_0}. \end{aligned} \tag{5}$$

In the reduced system, the LO only contains the damping parameter c_1, while the LVA and the NES have three (ε, c_2, and k_s) and four (ε, c_2, k_s, and l_1) independent parameters, respectively. They correspond to the mass ratio, damping, spring stiffness, and geometry parameter of the absorber.

When $|x_1-x_2+l_2|<l_1$, Eq. (4) can be converted into the dimensionless polynomial equations by using the Taylor series:

$$\begin{aligned}
&\ddot{x}_1 + c_1\dot{x}_1 + x_1 + c_2\left(\dot{x}_1 - \dot{x}_2\right) + 2k_s\left(1 - \frac{1}{l_1}\right)\left(x_1 - x_2 + l_2\right) + \frac{k_s}{l_1^3}\left(x_1 - x_2 + l_2\right)^3 + f_0\cos\left(\omega t\right) = 0,\\
&\varepsilon\ddot{x}_2 + c_2\left(\dot{x}_2 - \dot{x}_1\right) - 2k_s\left(1 - \frac{1}{l_1}\right)\left(x_1 - x_2 + l_2\right) - \frac{k_s}{l_1^3}\left(x_1 - x_2 + l_2\right)^3 = 0.
\end{aligned} \tag{6}$$

where Eq. (6) keeps the first two terms of the Taylor series. From Eq. (4), it can be seen that the geometry parameter l_1 determines the property of the NES ($0<l_1<1$ for the bistable NES with negative linear stiffness, $l_1=1$ for the monostable NES with zero linear stiffness, and $l_1>1$ for the NVA with positive linear stiffness). The potential energy surfaces reflecting the characteristics of these three NVAs can be found in Ref. [17]. For the bistable NES, the smaller l_1 is, the deeper the potential wells are. For the NVA with positive linear stiffness, the larger l_1 is, the stronger the positive linear stiffness is. Since the square root model of Eq. (4) can better describe global dynamic behaviors and the previous study proves the distortion of the potential energy surface and nonlinear normal modes caused by the polynomial model of Eq. (6) [17], this paper will adopt Eq. (4) to compute the response of the LO-NES system.

Back to Eq. (3), the exact solutions of the LO-LVA system can be computed. The steady-state general solutions are assumed as

$$x_1 = B_1\sin\left(\omega t\right) + B_2\cos\left(\omega t\right), x_2 = B_3\sin\left(\omega t\right) + B_4\cos\left(\omega t\right). \tag{7}$$

Substituting Eq. (7) into Eq. (3), and setting the coefficients of $\sin(\omega t)$ and $\cos(\omega t)$ as 0, the expressions of the amplitudes B_1~B_4 can be obtained, and the steady-state displacement amplitudes of the LO and the LVA (A_{LO} and A_{LVA}) can be computed by

$$A_{\mathrm{LO}} = \sqrt{B_1^2 + B_2^2}, A_{\mathrm{LVA}} = \sqrt{B_3^2 + B_4^2}. \tag{8}$$

Then the optimization of the LO-LVA system can be easily conducted. However, the exact solutions are hard to be computed in the LO-NES system. In previous studies, the steady-state responses of the LO-NES system can be approximately analyzed by the slow invariant manifold [26], the complexification-averaging method [38], and the harmonic balance method [39]. Yet the time history and amplitudes of aperiodic responses, e.g. strongly modulated response and chaos, cannot be well predicted by these methods, while the Runge-Kutta method (a common way of numerical simulation) can. Therefore, this paper will use the results of the Runge-Kutta method to optimize the LO-NES system.

In this paper, the damping value of the LO c_1 will be constantly set as 0.2. The parameter

optimization ranges of the absorber are $10^{-7}\leq\varepsilon\leq0.02$, $10^{-7}\leq c_2\leq10$, $10^{-7}\leq k_s\leq20$, and $10^{-7}\leq l_1\leq2$. The results of the Runge-Kutta method will be computed in 100 periods, and the last 20-period results will be left for computing the steady-state amplitudes. The time step is 1/200 of a period. In all the excitation conditions, the initial values of displacement and velocity are 0, and the range and step size of the excitation frequency ω are 0.8~1.2 and 0.02, respectively.

3 Single-objective functions and differential evolutionary algorithm

Since real structures may be excited in fixed or varied frequency, this paper will study the optimization issue of the LO-LVA and LO-NES systems in single- and sweep-frequency excitation conditions. As the main purpose of adding vibration absorber is to reduce the amplitude of the main system as much as possible, the single-objective function (SOF) will be set as $\min(A_{LO})$ and $\min(\max(A_{LO}))$ in single- and sweep-frequency excitation conditions, respectively. Although the introduction of the absorber can mitigate the vibration of the main system, the amplitude of the absorber may be quite large. Therefore, by considering the maximum amplitude of the whole system, the SOF will also be set as $\min(\max(A_{LO}, A_{LVA} \text{ or } A_{NES}))$, where A_{NES} denotes the displacement amplitude of the NES. In brief, this paper will study four types of SOFs in Table 1. The decay rate of the target amplitude relative to the original LO amplitude (without the absorber) can be calculated in each SOF. Then the amplitude decay rate can be used to evaluate the vibration mitigation effects of the LVA and the NES in different objective and excitation conditions.

Table 1 Four single-objective functions.

Abbreviation	Objective function	Excitation condition	Amplitude decay rate
SOF-1	$\min(A_{LO})$	single-frequency	$R_{A,1}$
SOF-2	$\min[\max(A_{LO}, A_{LVA} \text{ or } A_{NES})]$	single-frequency	$R_{A,2}$
SOF-3	$\min(\max(A_{LO}))$	sweep-frequency	$R_{A,3}$
SOF-4	$\min[\max(A_{LO}, A_{LVA} \text{ or } A_{NES})]$	sweep-frequency	$R_{A,4}$

The DE algorithm is often used to search for the optimal solution of nonlinear and non-differentiable problems and has the advantage of fast convergence and high robustness [40]. Here, the DE algorithm is used to optimize the parameters of the LVA and the NES in four single-objective optimization situations. The procedure of the single-objective DE algorithm is as follows:

(i) Initialization: The initial population $[u_1(i, 0), u_2(i, 0),\ldots, u_D(i, 0)]$ denoting the values of ε, c_2, k_s, and l_1 are randomly generated within the thresholds. D is the dimension of tuning parameters. For the LVA, D=3; for the NES, D=4. i is the population number. $1\le i\le M$, where M is the population size.

(ii) Mutation: In the jth iteration, three different members (number r_1, r_2, and r_3) except the ith member are randomly selected in the population to generate the ith mutant member. The expression is

$$v_k(i,j)=u_k(r_1,j)+F\left[u_k(r_2,j)-u_k(r_3,j)\right],1\le k\le D, j\ge 0, \tag{9}$$

where F is the scale factor and satisfies the uniform distribution on the interval $[-2,2]$. Small and large absolute values of F are beneficial to searching the local and global optima, respectively.

(iii) Crossover: The mixed member $\boldsymbol{w}(i, j)$ is obtained by mixing the original member $\boldsymbol{u}(i, j)$ and the mutant member $\boldsymbol{v}(i, j)$. The mixing rule is

$$w_k(i,j)=\begin{cases} v_k(i,j), & \text{if } r_4\le c_r \text{ or } k=I_r \\ u_k(i,j), & \text{otherwise} \end{cases}, \tag{10}$$

where r_4 is a random number uniformly distributed on the interval [0,1]. c_r is the crossover probability. The greater c_r is, the more information of the original member will be replaced by the mutant member. To replace the information of the original member as much as possible, c_r is set as 0.9. I_r is a random integer of 1~D and is used to make the mixed member and the original member differ in at least one dimension.

(iv) Selection: Comparing the values of the single-objective function of the original member $\boldsymbol{u}(i, j)$ and the mixed member $\boldsymbol{w}(i, j)$, the optimal one will be left as the original member $\boldsymbol{u}(i, j+1)$ in the next iteration. If j is smaller than the maximum iteration j_{max}, then $j=j+1$ and back to Step (ii). Otherwise, the trial is over.

Since the single-objective DE algorithm converges to the global optimal solution with a certain probability [41, 42], 20 trials are carried out on the same optimization problem to search for the optimal result. Through convergence verification, the population size M and the maximum iteration j_{max} of the single-objective DE algorithm are set as 40 and 100, respectively. The results of the single-objective DE algorithm are also verified by the parameter sensitivity analysis.

4 Numerical examples of single-objective optimization

4.1 Results of the DE algorithm in single-frequency excitation conditions

In this subsection, the results of SOF-1 and SOF-2 of the LO-NES system will be first presented. Then the comparison between the LVA and the NES will be conducted. Fig. 3 shows the objective results of the LO-NES system. For the SOF-1 in Fig. 3(a) and Fig. 3(c), the amplitude of the LO can be almost 100% attenuated in a broad excitation frequency and strength range, but the amplitude of the NES exceeds the original amplitude of the LO. For the SOF-2 in Fig. 3(b) and Fig. 3(d), the best vibration mitigation effect can be found when the excitation frequency is close to the resonance frequency of the LO (ω=1). At this moment, the LO and the NES have the same optimal amplitudes, and the excitation strength f_0 hardly changes the vibration mitigation effect as well.

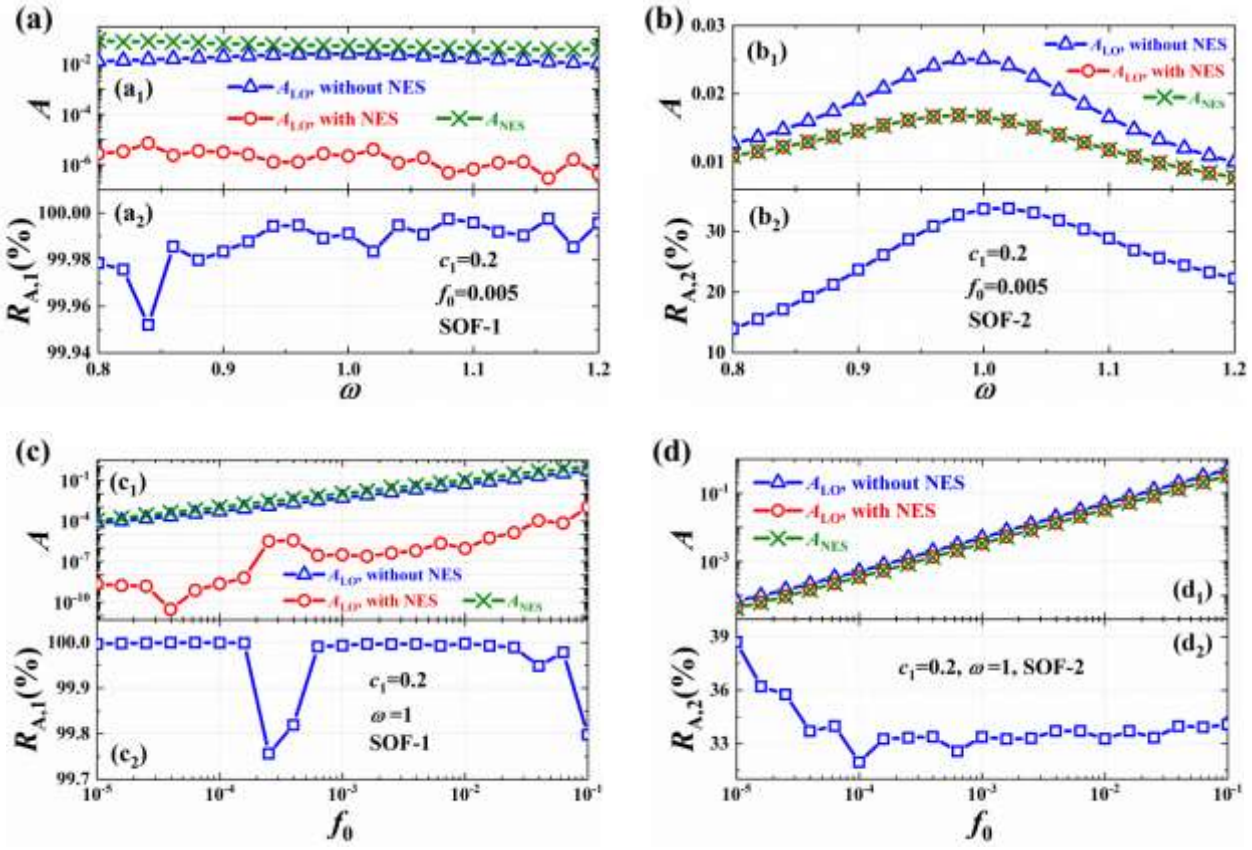

Fig. 3. Amplitudes of the LO and the NES and amplitude decay rate in different objective and single-frequency excitation conditions: (a) and (b) SOF-1 & SOF-2, f_0=0.005, ω=0.8~1.2; (c) and (d) SOF-1 & SOF-2, ω=1, lg(f_0)=−5~−1.

Corresponding to the optimization results of amplitude decay rate in Fig. 3, Fig. 4 and Table 2 present the results of four optimized parameters of the NES. It can be seen that all the values of the optimized mass ratio ε are close to its upper limit (10%), which indicates better vibration mitigation

effects prefer larger mass of the NES. For the values of the optimized damping c_2, differences can be found in the SOF-1 and the SOF-2. That is, the values of c_2 are very close to 0 in the SOF-1. Combined with the results of Fig. 3(a) and Fig. 3(c), the NES exhibits anti-resonance characteristics similar to those of the undamped LVA in the SOF-1. In the SOF-2, most values of c_2 are confined in the range 0.01~1, and the value of c_2 will not be affected by f_0 but will increase when ω increases. For the optimized spring stiffness k_s, most values are confined in the range 0.01~10. For the optimized geometry parameter l_1, most values are larger than 1, which corresponds to the NVA with positive linear stiffness. These tuning parameter results will help to the practical design of the NES in single-frequency excitation conditions.

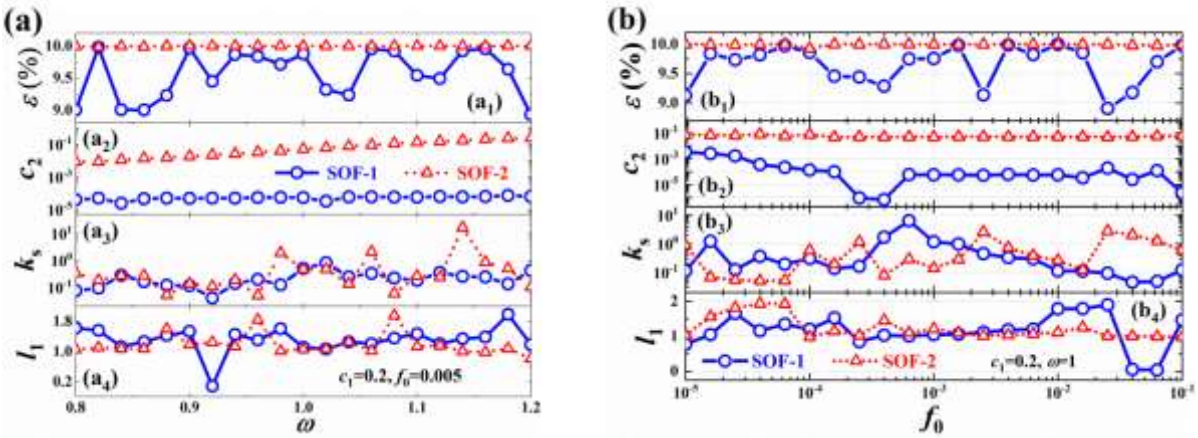

Fig. 4. Optimal parameters of the NES in different objective and single-frequency excitation conditions: (a) SOF-1 & SOF-2, f_0=0.005, ω=0.8~1.2; (b) SOF-1 & SOF-2, ω=1, lg(f_0)=−5~−1.

Table 2 Mean values of optimal parameters of the NES in different objective and single-frequency excitation conditions.

Excitation condition	Objective function	ε_{mean}	$c_{2,mean}$	$k_{s,mean}$	$l_{1,mean}$
f_0=0.005, ω=0.8~1.2	SOF-1	0.0956	5.4×10^{-5}	0.2400	1.3084
f_0=0.005, ω=0.8~1.2	SOF-2	0.1000	0.0819	1.1910	1.1796
ω=1, lg(f_0)=-5~-1	SOF-1	0.0965	4.3×10^{-4}	0.6891	1.1499
ω=1, lg(f_0)=-5~-1	SOF-2	0.0999	0.0558	0.6956	1.2228

In the SOF-1, the optimal NES is similar to the undamped LVA. What about the similarities and disparities of the optimal NES and the optimal LVA in the SOF-2? The results in Table 3 show that the optimal NES and the optimal LVA have almost the same values of the mass ratio ε, the damping c_2, and the amplitude decay rate $R_{A,2}$ (vibration mitigation effect) in different excitation conditions. Besides, both the NVA with positive linear stiffness (l_1>1) and the bistable NES (l_1<1)

can achieve the optimal control of the LO and the absorber, and the differences in the optimized values of the geometry parameter l_1 will cause those of the NES spring stiffness k_s.

Table 3 Optimal parameters, the LO amplitude, and amplitude decay rate of the LO-LVA and LO-NES systems in the SOF-2 and different single-frequency excitation conditions.

Absorber	f_0	ω	ε	c_2	k_s	l_1	A_{LO}	A_{LVA} or A_{NES}	$R_{A,2}(\%)$
LVA	0.005	1	0.1	0.05	0.05	-	0.0167	0.0167	33.44
NES	0.005	1	0.1	0.0497	0.1124	1.2858	0.0166	0.0166	33.84
NES	0.005	1	0.1	0.0516	0.4806	1.0547	0.0166	0.0166	33.84
LVA	0.005	0.8	0.1	0.0085	0.0320	-	0.0109	0.0109	13.97
NES	0.005	0.8	0.1	0.0077	0.0344	1.8675	0.0109	0.0109	13.97
NES	0.005	0.8	0.1	0.0070	0.1289	1.1411	0.0109	0.0109	13.97
LVA	0.005	1.2	0.1	0.2353	0.0720	-	0.0077	0.0077	22.86
NES	0.005	1.2	0.1	0.2591	0.9384	0.9808	0.0078	0.0078	21.86
NES	0.005	1.2	0.1	0.2403	0.2700	1.1541	0.0078	0.0078	21.86
LVA	0.1	1	0.1	0.05	0.05	-	0.3333	0.3333	33.44
NES	0.1	1	0.1	0.0533	0.4766	0.9785	0.3308	0.3308	34.05
NES	0.1	1	0.1	0.0534	0.4611	0.9809	0.3308	0.3308	34.05

4.2 Results of the DE algorithm in sweep-frequency excitation conditions

Subsection 4.1 presents the results of the global control of the system and the similarities and disparities of the optimal NES and the optimal LVA in single-frequency excitation conditions. Here, the authors focus on sweep-frequency excitation conditions (SOF-3 & SOF-4). The results are shown in Table 4 and Table 5. Decent vibration mitigation effects can be witnessed in the SOF-3 and the SOF-4. Since the SOF-4 includes the control of the amplitude of the absorber, the optimal amplitude decay rate in Table 5 is not up to that of the SOF-3 in Table 4. However, the value of $R_{A,4}$ in Table 5 is very close to the value of $R_{A,2}$ with ω=1 in Table 3, which indicates the similar global control effects in both single- and sweep-frequency excitation conditions. Besides, for the optimal NES and the optimal LVA, the similarities can be found in the mass ratio, the damping, and the vibration mitigation effect in Table 4 and Table 5. Yet all the results of the geometry parameter l_1 are larger than 1, which may cause some misunderstanding that only the NVA with positive linear stiffness can achieve the optimal vibration mitigation effect in the sweep-frequency excitation condition. Since the optimal parameter combinations of the NES are not unique, and the DE algorithm easily converges to certain positions (like l_1>1) but misses some other important

information (like the bistable situation with l_1<1) in the parameter space, other approaches are needed to capture this important information.

Table 4 Optimal parameters, the LO maximum amplitude, and amplitude decay rate of the LO-LVA and LO-NES systems in the SOF-3 and different excitation strength conditions.

Absorber	f_0	ε	c_2	k_s	l_1	max(A_{LO})	max(A_{LVA} or A_{NES})	$R_{A,3}$(%)
LVA	0.005	0.1	0.0343	0.0743	-	0.0131	0.0354	47.79
NES	0.005	0.1	0.0332	0.1429	1.3511	0.0131	0.0362	47.79
NES	0.005	0.1	0.0329	0.3969	1.1030	0.0131	0.0364	47.79
LVA	0.1	0.1	0.0343	0.0743	-	0.2618	0.7079	47.81
NES	0.1	0.1	0.0339	0.0741	1.9397	0.2618	0.7156	47.81
NES	0.1	0.1	0.0375	0.1471	1.2475	0.2645	0.6807	47.27

Table 5 Optimal parameters, the LO maximum amplitude, and amplitude decay rate of the LO-LVA and LO-NES systems in the SOF-4 and different excitation strength conditions.

Absorber	f_0	ε	c_2	k_s	l_1	max(A_{LO})	max(A_{LVA} or A_{NES})	$R_{A,4}$(%)
LVA	0.005	0.1	0.0447	0.0459	-	0.0172	0.0172	31.45
NES	0.005	0.1	0.0452	0.0962	1.3114	0.0172	0.0171	31.45
NES	0.005	0.1	0.0462	0.1637	1.1621	0.0172	0.0171	31.45
LVA	0.1	0.1	0.0447	0.0459	-	0.3443	0.3443	31.45
NES	0.1	0.1	0.0462	0.0449	1.9985	0.3431	0.3431	31.60
NES	0.1	0.1	0.0435	0.2266	1.0280	0.3424	0.3424	31.74

4.3 Results of the parameter sensitivity analysis

In Subsection 4.1 and 4.2, the parameters and amplitude decay rates of the optimal LVA and the optimal NES are obtained by the DE algorithm in different objective and excitation conditions. However, it is very difficult to achieve the optimal vibration mitigation effect due to the influence of parameter uncertainty and manufacturing error in practical engineering. So the parameter range to achieve decent vibration mitigation effects needs to be found out. Combined with the above DE algorithm results and the parameter sensitivity analysis, this task can be well accomplished, and more differences in the parameter design of the absorbers may appear. According to the results in Table 3, Table 4, and Table 5, this subsection will present the influences of the absorber parameters on the vibration mitigation effect in three SOFs and two excitation strength conditions (f_0=0.005 or 0.1). The mass ratio ε of the absorbers will be set as 0.1 (the upper limit value).

Fig. 5 and Fig. 6 show the results of the amplitude decay rates of the LO-LVA and LO-NES

systems by the parameter sensitivity analysis. Firstly, in Fig. 5, it can be seen that the LVA can only achieve decent vibration mitigation effects when the spring stiffness k_s is less than 0.2, while in Fig. 6, the effectiveness of the NES can be discovered when the spring stiffness k_s is larger than 0.4. This reveals the better stiffness robustness of the NES versus the LVA in vibration mitigation. Secondly, the results of small excitation strength (f_0=0.005) in Fig. 6(a), (b), and (c) indicate that both the NVA with positive linear stiffness (l_1>1) and the bistable NES (l_1<1) can achieve decent vibration mitigation effects, and the closer the NES is to the monostable state (the dashed line l_1=1), the larger the effective stiffness range will be. The results of large excitation strength (f_0=0.1) in Fig. 6(d), (e), and (f) indicate that the bistable NES cannot achieve decent vibration mitigation effects within a large geometry parameter range (the range between the two dashed lines). The results in Fig. 6 also show the significant effect of the excitation strength on the effective parameter range of the NES, which is significantly different from that of the LVA. Thirdly, the results of parameter sensitivity analysis in Fig. 5 and Fig. 6 can well verify the results of the DE algorithm in Table 3, Table 4, and Table 5. On the other hand, the parameter sensitivity analysis can more comprehensively reflect the optimal parameter range of the NES than the DE algorithm, especially the bistable NES.

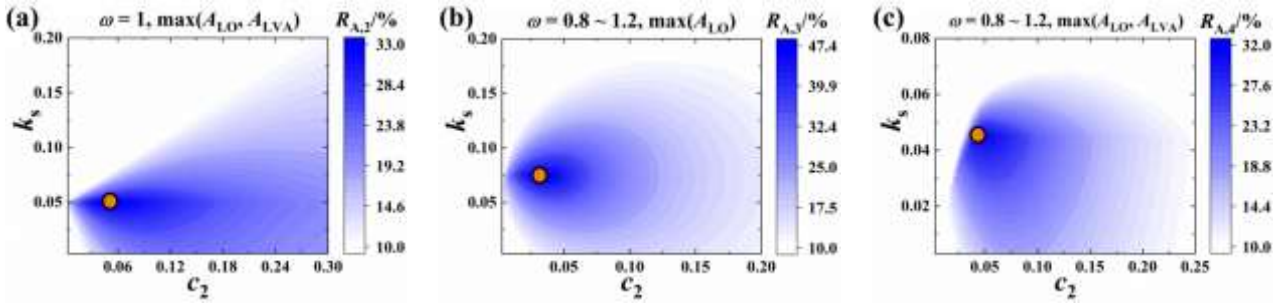

Fig. 5. Amplitude decay rates of the LO-LVA system with f_0=0.005 or 0.1, ε=0.1, and varied damping c_2, spring stiffness k_s, and SOFs, where the circles denote the results of the DE algorithm: (a) SOF-2; (b) SOF-3; (c) SOF-4.

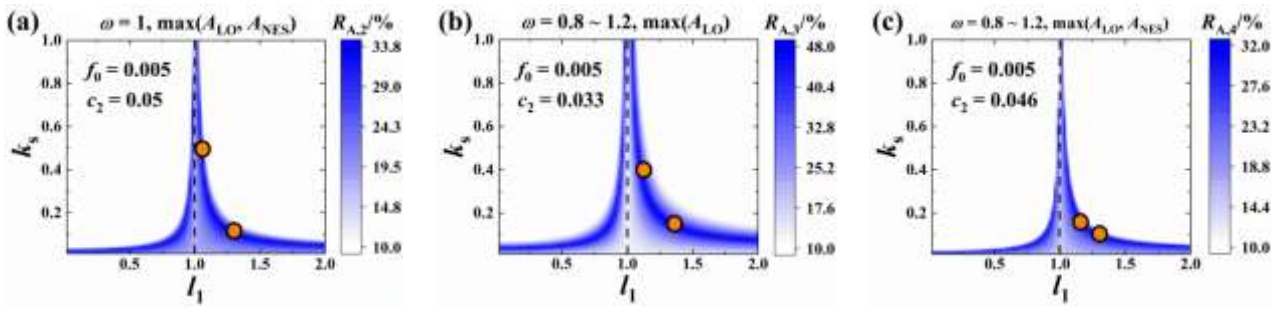

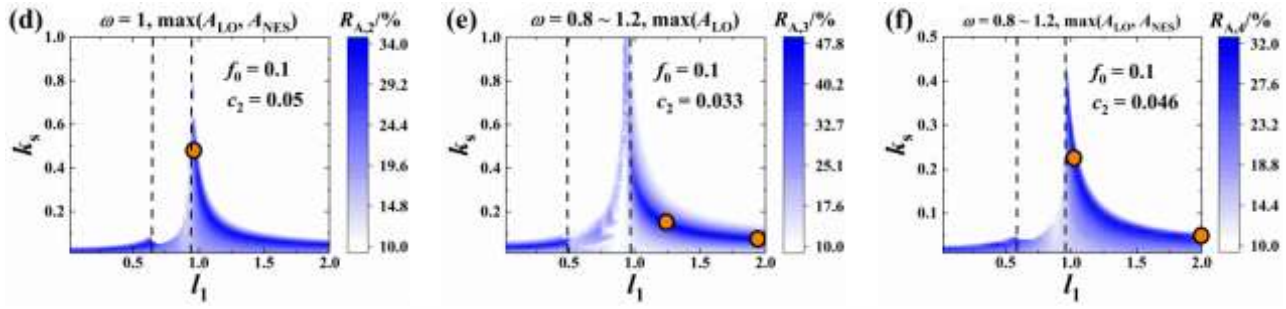

Fig. 6. Amplitude decay rates of the LO-NES system with f_0=0.005 or 0.1, ε=0.1, optimal damping c_2, and varied spring stiffness k_s, geometry parameter l_1, and SOFs, where the circles denote the results of the DE algorithm: (a) and (d) SOF-2; (b) and (e) SOF-3; (c) and (f) SOF-4.

In Fig. 5 and Fig. 6, the effective combinations of the spring stiffness k_s and the geometry parameter l_1 are searched in the optimal damping condition. These results show that the NES can achieve decent vibration mitigation effects within a wide range of the geometry parameter. Then, among the bistable NES, the monostable NES (l_1=1), or the NVA with positive linear stiffness, which type of the NVA has a wider effective parameter range? Taking the monostable NES as a reference, the bistable NES with l_1=0.99 and the NVA with l_1=1.01 are selected to compute the results of amplitude decay rates in different SOF and excitation conditions, and the effective ranges of the damping c_2 and the spring stiffness k_s are found, as shown in Fig. 7, Fig. 8, Fig. 9, and Table 6. It can be seen that, in most cases, the vibration mitigation effect of the NES is decided by both the damping and the spring stiffness, while that of the monostable NES in Fig. 7(b), Fig. 8(b), and Fig. 9(b) is basically independent of its spring stiffness in small excitation (f_0=0.005). In this situation, the monostable NES has optimal stiffness robustness. Since the dynamic equation of the monostable NES can be converted into the form of zero linear stiffness and cubic nonlinear stiffness by Taylor series in small excitation, the monostable NES does not need tuning stiffness to achieve the optimal vibration mitigation. However, the vibration mitigation effect of the optimal monostable NES (the upper limit value of the amplitude decay rate) is inferior to the optimal LVA, the optimal bistable NES, and the optimal NVA with positive linear stiffness. In large excitation, the solution of the dynamic equation is not in the convergence domain of Taylor series because of the large response of the system. At this time, the monostable NES does not have the characteristics of zero linear stiffness, and tuning stiffness is needed to achieve optimal vibration mitigation. That is also why the results of parameter analysis of the monostable NES in large excitation are very close to those of the bistable NES and the NVA with positive linear stiffness. In addition, the results in Fig. 7, Fig. 8, Fig. 9, and Table 6 indicate the optimal stiffness robustness of the bistable NES among the

three types of the NVA in large excitation. Since the NES has a linear damping structure, the NES also needs tuning damping to realize the optimal vibration mitigation, and the effective range of the damping c_2 of the three NVAs is almost the same as that of the LVA.

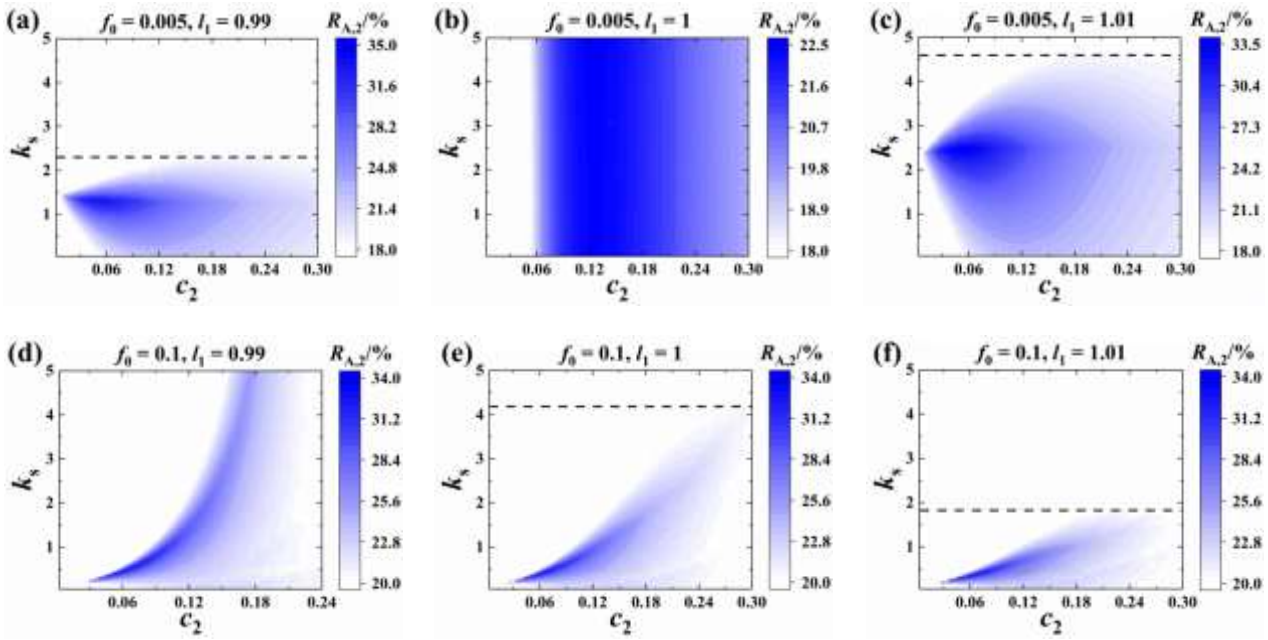

Fig. 7. Amplitude decay rate $R_{A,2}$ of the LO-NES system with f_0=0.005 or 0.1, ε=0.1, and varied damping c_2, spring stiffness k_s, geometry parameter l_1 in the SOF-2, where the dashed lines denote the upper limit values of effective k_s: (a) and (d) the bistable NES with l_1=0.99; (b) and (e) the monostable NES with l_1=1; (c) and (f) the NVA with l_1=1.01.

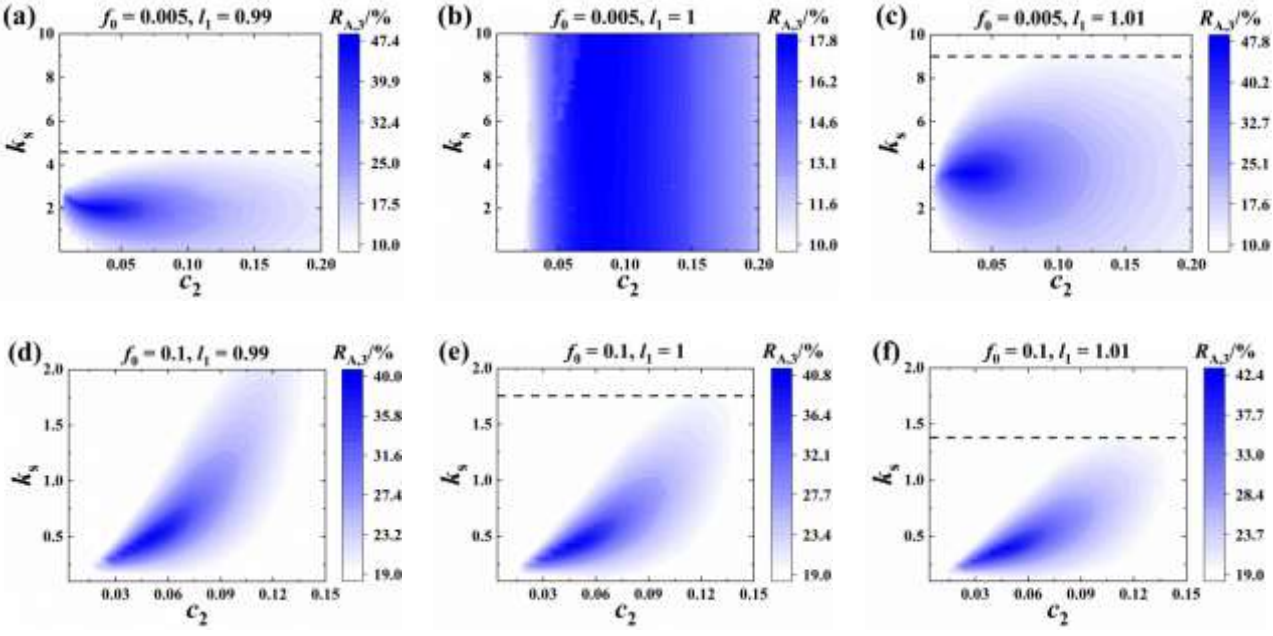

Fig. 8. Amplitude decay rate $R_{A,3}$ of the LO-NES system with f_0=0.005 or 0.1, ε=0.1, and varied damping c_2, spring stiffness k_s, geometry parameter l_1 in the SOF-3, where the dashed lines denote the upper limit values of effective k_s: (a) and (d) the bistable NES with l_1=0.99; (b) and (e) the monostable NES with l_1=1; (c) and (f) the NVA with l_1=1.01.

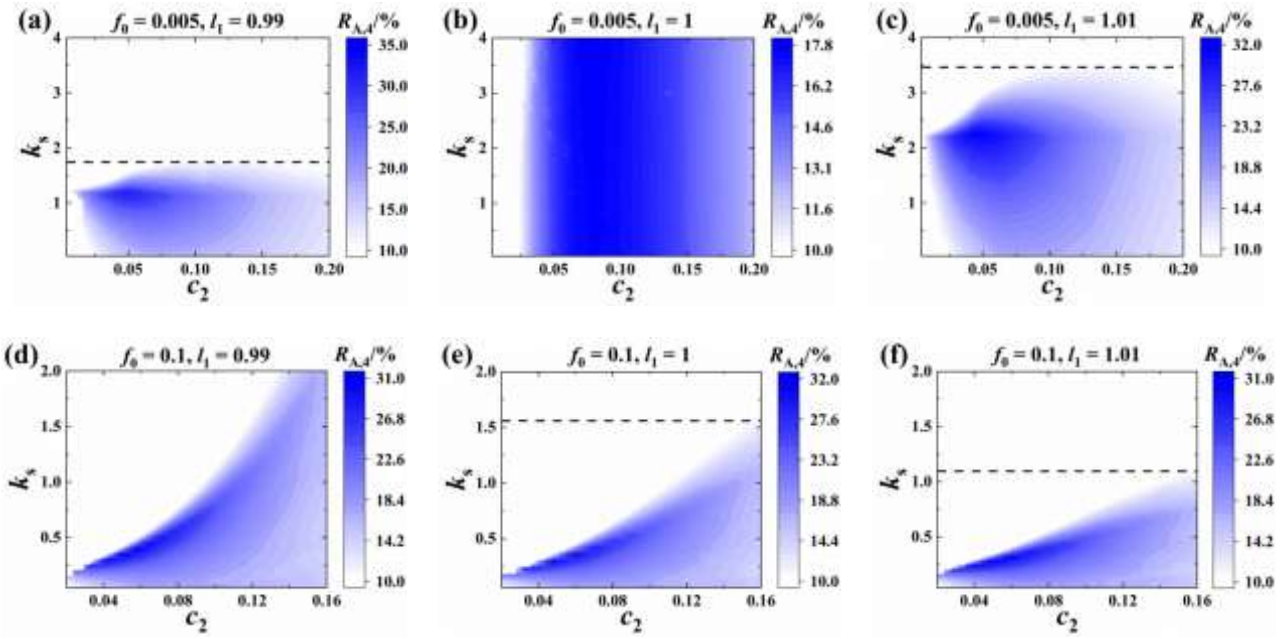

Fig. 9. Amplitude decay rate $R_{A,4}$ of the LO-NES system with f_0=0.005 or 0.1, ε=0.1, and varied damping c_2, spring stiffness k_s, geometry parameter l_1 in the SOF-4, where the dashed lines denote the upper limit values of effective k_s: (a) and (d) the bistable NES with l_1=0.99; (b) and (e) the monostable NES with l_1=1; (c) and (f) the NVA with l_1=1.01.

Table 6 Upper limit values of effective spring stiffness of the NES in different SOF, excitation strength, and geometry conditions in Fig. 7, Fig. 8, and Fig. 9.

Objective function	f_0	**Lower limit of R_A (%)**	**Upper limit of R_A (%)**	l_1	**Upper limit of effective k_s**
SOF-2	0.005	18.0	35.0	0.99	2.3
SOF-2	0.005	18.0	22.5	1	>5
SOF-2	0.005	18.0	33.5	1.01	4.6
SOF-2	0.1	20.0	34.0	0.99	>5
SOF-2	0.1	20.0	34.0	1	4.2
SOF-2	0.1	20.0	34.0	1.01	1.8
SOF-3	0.005	10.0	47.4	0.99	4.6
SOF-3	0.005	10.0	17.8	1	>10
SOF-3	0.005	10.0	47.8	1.01	9
SOF-3	0.1	19.0	40.0	0.99	2
SOF-3	0.1	19.0	40.8	1	1.8
SOF-3	0.1	19.0	42.4	1.01	1.4
SOF-4	0.005	10.0	35.0	0.99	1.8
SOF-4	0.005	10.0	17.8	1	>4
SOF-4	0.005	10.0	32.0	1.01	3.5
SOF-4	0.1	10.0	31.0	0.99	>2
SOF-4	0.1	10.0	32.0	1	1.6

SOF-4	0.1	10.0	31.0	1.01	1.1

4.4 Frequency responses of the LO with the optimized absorber

The above three subsections present the similarities and disparities of the effective parameter combinations of the LVA and the NES in ε=0.1 and different objective and excitation conditions. So what are the similarities and disparities of their dynamic responses? This subsection will study this issue. Since the system in sweep-frequency excitation contains more dynamic behaviors than the system in single-frequency excitation, this subsection will focus on the frequency responses in the SOF-3 and the SOF-4.

Fig. 10 shows the results of frequency responses of the optimal LO-LVA and LO-NES systems and the optimized parameter values of the NES in the SOF-3. The results of small excitation (f_0=0.005) in Fig. 10(a), (b), and (c) show that the absorbers achieve the optimal vibration mitigation effect through periodic motion. Particularly, by comparing the amplitude of the optimal bistable NES and the distance between its two unstable equilibrium positions ($2l_2$), it is found that the dynamic response of the optimal bistable NES is the local (in-well) periodic motion. In addition, the weakness of the NES nonlinear stiffness in small excitation makes the optimal LVA, the optimal bistable NES (l_1=0.9), and the optimal NVA with positive linear stiffness (l_1=1.01) have the same tuning features. These tuning features are the variation of the resonance frequency of the LO, two flat equivalent peaks of the frequency response of the LO, and large low-frequency responses of the NES which exceeds the maximum amplitude of the original LO. For the optimal monostable NES (l_1=1), according to the analysis in Subsection 4.3, there are no characteristics of tuning stiffness in small excitation, so it will maintain the single-peak characteristics of the frequency response and not greatly change the resonance frequency of the LO. However, due to the small response of the monostable NES, the vibrational energy cannot be optimally transferred from the LO to the monostable NES.

Since the results in Fig. 6 imply the poor performance of the bistable NES in a large range of geometry parameter l_1 in large excitation, the authors seek for the explanation by comparing the frequency responses and the optimized parameter values of the optimal bistable deep-well NES (l_1=0.9), the optimal bistable shallow-well NES (l_1=0.99), and the optimal monostable NES (l_1=1). The results in Fig. 10(d) show that the optimal damping value of the bistable deep-well NES differs from those of the bistable shallow-well NES and the monostable NES, and the bistable deep-well

NES system has six kinds of responses in the whole frequency domain in large excitation (f_0=0.1). Numbers 1~6 in Fig. 10(d) correspond to the local periodic motion (LPM), the chaos dominated by in-well motion (Chaos-1), the global periodic motion dominated by the excitation frequency (GPM-1), the strongly modulated response (SMR), the chaos dominated by cross-well motion (Chaos-2), and the global periodic motion dominated by the low-frequency component (GPM-2) in Fig. 11(a)~(f). Compared with the results of the periodic response in Fig. 10(e) and (f), the aperiodic response in Fig. 10(d) leads to the larger amplitude of the LO, which is not conducive to vibration mitigation. In addition, because of the great effect of the NES nonlinear stiffness in large excitation, the frequency responses of the optimal LO-NES system have different resonance frequencies versus the optimal LO-LVA system. Since the optimal monostable NES does not have the characteristics of zero linear stiffness in large excitation, its frequency response is consistent with that of the optimal bistable shallow-well NES.

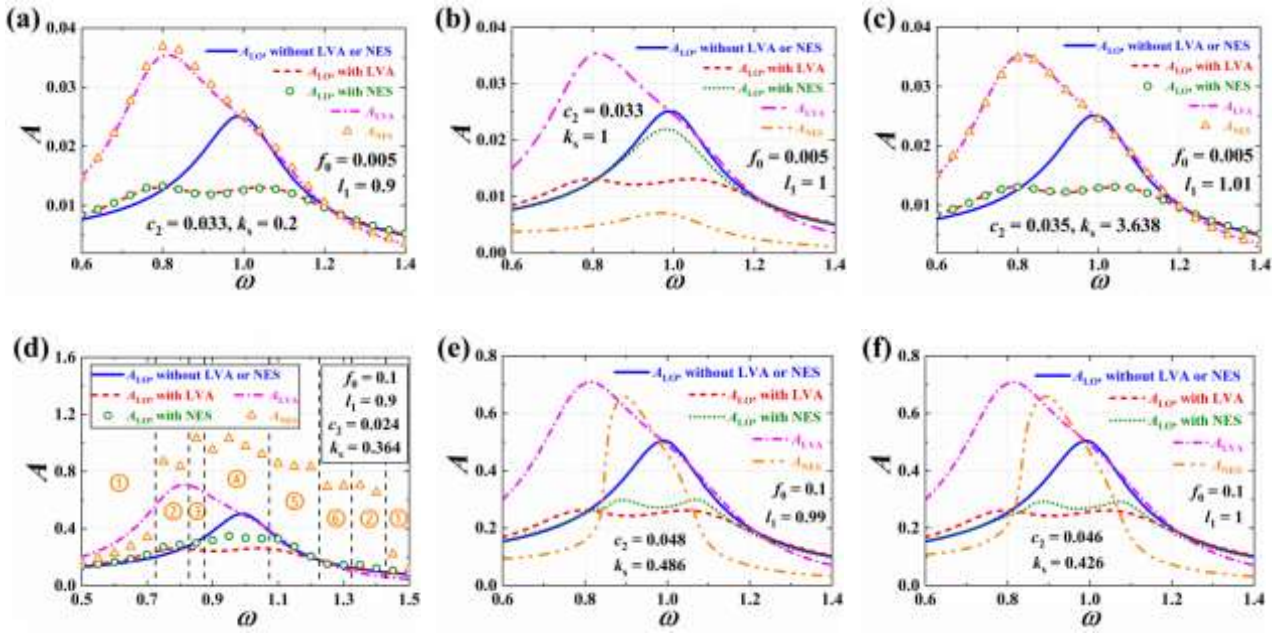

Fig. 10. Frequency responses of the LO coupled with the optimal LVA or the optimal NES in different excitation and geometry conditions, ε=0.1, and the SOF-3: (a) f_0=0.005, l_1=0.9; (b) f_0=0.005, l_1=1; (c) f_0=0.005, l_1=1.01; (d) f_0=0.1, l_1=0.9; (e) f_0=0.1, l_1=0.99; (f) f_0=0.1, l_1=1.

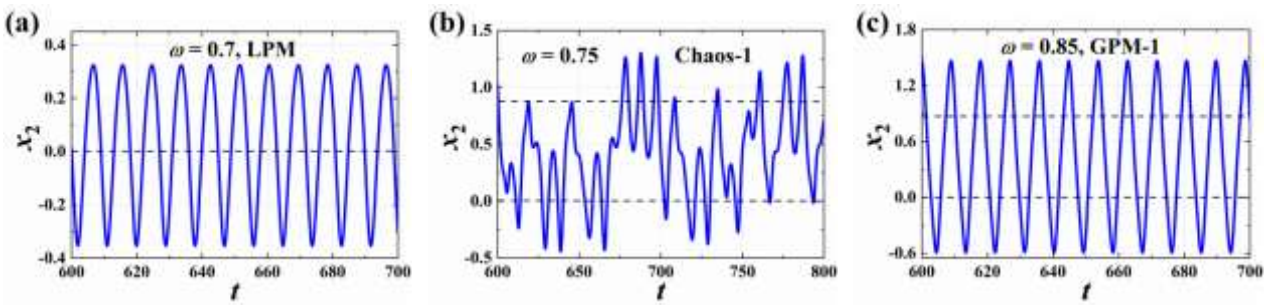

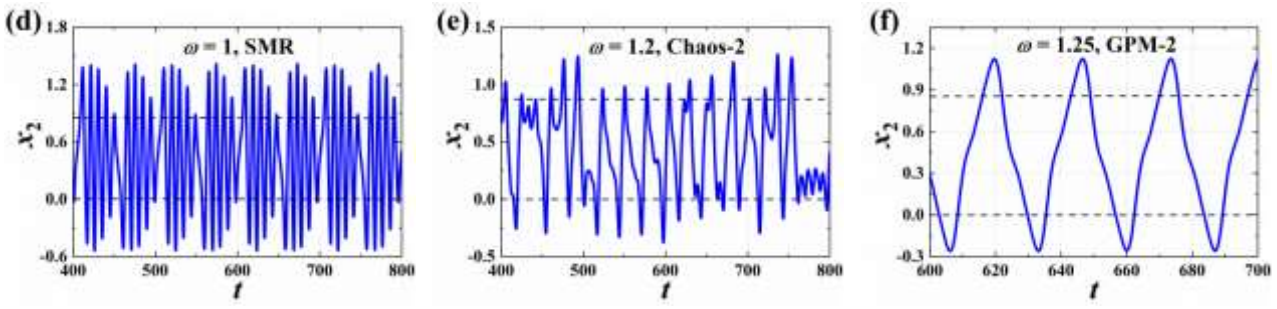

Fig. 11. Displacement time histories of the bistable NES in different excitation frequency conditions in Fig. 10(d): (a) local periodic motion with ω=0.7; (b) chaos dominated by in-well motion with ω=0.75; (c) global periodic motion dominated by excitation frequency with ω=0.85; (d) strongly modulated response with ω=1; (e) chaos dominated by cross-well motion with ω=1.2; (f) global periodic motion dominated by low-frequency component with ω=1.25.

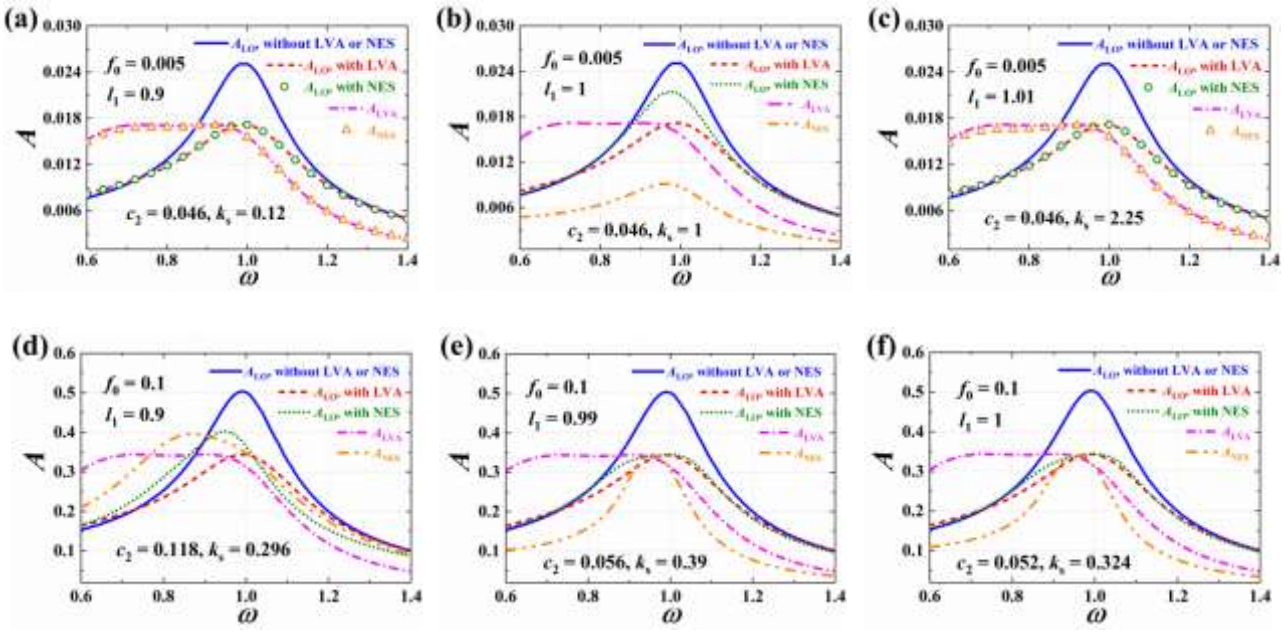

Fig. 12. Frequency responses of the LO coupled with the optimal LVA or the optimal NES in different excitation and geometry conditions, ε=0.1, and the SOF-4: (a) f_0=0.005, l_1=0.9; (b) f_0=0.005, l_1=1; (c) f_0=0.005, l_1=1.01; (d) f_0=0.1, l_1=0.9; (e) f_0=0.1, l_1=0.99; (f) f_0=0.1, l_1=1.

Compared with the results of only suppressing the amplitude of the LO (SOF-3) in Fig. 10, the results of suppressing both the amplitudes of the LO and the absorber (SOF-4) in Fig. 12 prevent the large amplitude of the absorber at low frequency and does not change the resonance frequency and single-peak characteristics of the LO. This indicates the great advantages and application potential of the global control strategy in vibration mitigation. Besides, in Fig. 12(e) and (f), affected by the nonlinear stiffness, the frequency responses of the optimal bistable shallow-well NES (l_1=0.99) and the optimal monostable NES (l_1=1) are smaller than that of the optimal LVA and also maintain the single-peak characteristics in large excitation, which indicates the possible better

performance of the NES than the LVA in the global control. Although the optimal bistable deep-well NES (l_1=0.9) does not produce aperiodic responses in Fig. 12(d), its vibration mitigation effect still cannot reach that of the optimal bistable shallow-well NES and the optimal monostable NES in Fig. 12(e) and (f) due to the difference of the optimal damping values.

5 Multi-objective functions and differential evolutionary algorithm

Sections 3 and 4 use the steady-state displacement amplitude to optimize the parameters of the absorbers. To fully display the vibration mitigation effect of the absorbers, researchers often examine multiple indexes, such as transmissibility and energy indexes [17, 27, 28]. Besides, not only mitigation effects but economic factors need considering in the design of the absorbers [30]. For example, Wang et al. took the displacement, damping force, and restoring force of the absorbers as the indexes of economic factors [30]. In fact, the economic factors also depend on the mass of the absorber; that is, manufacturing and maintenance costs will increase as the mass of the absorber increases. On the other hand, the previous study [17] and the above single-objective optimization results show that the larger the mass of the absorber, the more conducive to vibration mitigation. Therefore, the mass of the absorber is a very important index, and the parameter design of the absorber may differ in different requirements of the mass and the vibration mitigation effect. Therefore, the following content of this paper will present the multi-objective and multi-parameter design of the absorbers by taking the mass ratio ε and multiple vibration mitigation indexes as objective functions and using the multi-objective DE algorithm.

Combined with the amplitude index, the mechanical energy and the input energy of the system will also be adopted for evaluating the vibration mitigation performance. Taking the LO-NES system as an example, the expressions of the kinetic energy ($E_{\mathrm{ki,LO}}$ & $E_{\mathrm{ki,NES}}$), the potential energy ($E_{\mathrm{po,LO}}$ & $E_{\mathrm{po,NES}}$), the dissipated energy ($E_{\mathrm{di,LO}}$ & $E_{\mathrm{di,NES}}$), and the total energy ($E_{\mathrm{al,LO}}$ & $E_{\mathrm{al,NES}}$) are

$$\begin{aligned} &E_{\mathrm{ki,LO}}=\frac{\dot{x}_1^2}{2},E_{\mathrm{ki,NES}}=\frac{\varepsilon\dot{x}_2^2}{2},E_{\mathrm{po,LO}}=\frac{x_1^2}{2},E_{\mathrm{po,NES}}=k_{\mathrm{s}}\left[\sqrt{l_1^2+\left(x_1-x_2+l_2\right)^2}-1\right]^2,E_{\mathrm{di,LO}}=c_1\int_0^{t_{\mathrm{end}}}\dot{x}_1^2\mathrm{d}t,\\ &E_{\mathrm{di,NES}}=c_2\int_0^{t_{\mathrm{end}}}\left(\dot{x}_1-\dot{x}_2\right)^2\mathrm{d}t,E_{\mathrm{al,LO}}=E_{\mathrm{ki,LO}}+E_{\mathrm{po,LO}}+E_{\mathrm{di,LO}},E_{\mathrm{al,NES}}=E_{\mathrm{ki,NES}}+E_{\mathrm{po,NES}}+E_{\mathrm{di,NES}}, \end{aligned} \tag{11}$$

where $t_{\mathrm{end}}=200\pi/\omega$ and $\mathrm{d}t=\pi/(100\omega)$. Then the expressions of the mechanical energy ($E_{\mathrm{me,LO}}$ & $E_{\mathrm{me,NES}}$) for both the transient and steady-state processes and the input energy ($E_{\mathrm{in,LO}}$ & $E_{\mathrm{in,NES}}$) only for the steady-state process are

$$E_{\mathrm{me,LO}}=\frac{1}{t_{\mathrm{end}}}\int_0^{t_{\mathrm{end}}}\left(E_{\mathrm{ki,LO}}+E_{\mathrm{po,LO}}\right)\mathrm{d}t, E_{\mathrm{me,NES}}=\frac{1}{t_{\mathrm{end}}}\int_0^{t_{\mathrm{end}}}\left(E_{\mathrm{ki,NES}}+E_{\mathrm{po,NES}}\right)\mathrm{d}t,$$
$$E_{\mathrm{in,LO}}=\int_{t_{\mathrm{start}}}^{t_{\mathrm{end}}}\max\left[E_{\mathrm{al,LO}}(t)-E_{\mathrm{al,LO}}(t-\mathrm{d}t),0\right]\mathrm{d}t, E_{\mathrm{in,NES}}=\int_{t_{\mathrm{start}}}^{t_{\mathrm{end}}}\max\left[E_{\mathrm{al,NES}}(t)-E_{\mathrm{al,NES}}(t-\mathrm{d}t),0\right]\mathrm{d}t, \tag{12}$$

where $t_{\mathrm{start}}=160\pi/\omega$. Combining the mass ratio, the three mitigation performance measures, and the four SOFs in Table 1, this paper will study the optimization issues in four multi-objective functions (MOFs), as shown in Table 7. $A_{\max}$, $E_{\mathrm{me,max}}$, and $E_{\mathrm{in,max}}$ are the abbreviations of max(A_{LO}, A_{LVA} or A_{NES}), max($E_{\mathrm{me,LO}}$, $E_{\mathrm{me,LVA}}$ or $E_{\mathrm{me,NES}}$), and max($E_{\mathrm{in,LO}}$, $E_{\mathrm{in,LVA}}$ or $E_{\mathrm{in,NES}}$), respectively. $R_{\mathrm{me},1}$~$R_{\mathrm{me},4}$ and $R_{\mathrm{in},1}$~$R_{\mathrm{in},4}$ are the decay rate of the target mechanical and input energy relative to the original LO mechanical and input energy (without the absorber) in the four MOFs.

Table 7 Four multi-objective functions.

Abbreviation	Objective function	Excitation condition	Decay rate
MOF-1	min(ε), min(A_{LO}), min($E_{\mathrm{me,LO}}$), min($E_{\mathrm{in,LO}}$)	single-frequency	$R_{\mathrm{A},1}$, $R_{\mathrm{me},1}$, $R_{\mathrm{in},1}$
MOF-2	min(ε), min($A_{\max}$), min($E_{\mathrm{me,max}}$), min($E_{\mathrm{in,max}}$)	single-frequency	$R_{\mathrm{A},2}$, $R_{\mathrm{me},2}$, $R_{\mathrm{in},2}$
MOF-3	min(ε), min[max(A_{LO})], min[max($E_{\mathrm{me,LO}}$)], min[max($E_{\mathrm{in,LO}}$)]	sweep-frequency	$R_{\mathrm{A},3}$, $R_{\mathrm{me},3}$, $R_{\mathrm{in},3}$
MOF-4	min(ε), min($A_{\max}$), min($E_{\mathrm{me,max}}$), min($E_{\mathrm{in,max}}$)	sweep-frequency	$R_{\mathrm{A},4}$, $R_{\mathrm{me},4}$, $R_{\mathrm{in},4}$

The external archive and the non-dominated sorting are two common ways to deal with the multi-objective optimization problem [43, 44]. Accordingly, the flow charts of the multi-objective DE algorithms based on the external archive and the non-dominated sorting are shown in Fig. 13 and Fig. 14. In the external archive DE (EADE) algorithm, the population evolves in the same way as the single-objective DE algorithm, and the external archive is only used to store and update the non-dominated solutions. The non-dominated sorting DE (NSDE) algorithm firstly merges the parent population and the developed child population and then selects the optimal members as the new parent population through non-dominated sorting. During the iteration, the size of non-dominated solutions in the external archive or the non-dominated sorting group will continuously increase, so it is necessary to control the size of non-dominated solutions to ensure computational efficiency. For this purpose, the global density estimation method is adopted; that is to calculate the average distance of non-dominated solutions in the normalized target space and delete the crowded solutions in the external archive or the non-dominated sorting group. Setting the position of the rth non-dominated solution as $\boldsymbol{h}(r, j)$ and the size of the current external archive or non-dominated sorting group as R, the average distance d_r can be expressed as

$$d_r = (R-1) \Big/ \sum_{i=1, i\neq r}^{R} \frac{1}{\left\| \boldsymbol{h}(r,j) - \boldsymbol{h}(i,j) \right\|}, 1 \le r \le R,\ j \ge 0. \tag{13}$$

For convenience, the upper limit of the population size of the external archive or the non-dominated sorting group is set as the original population size M.

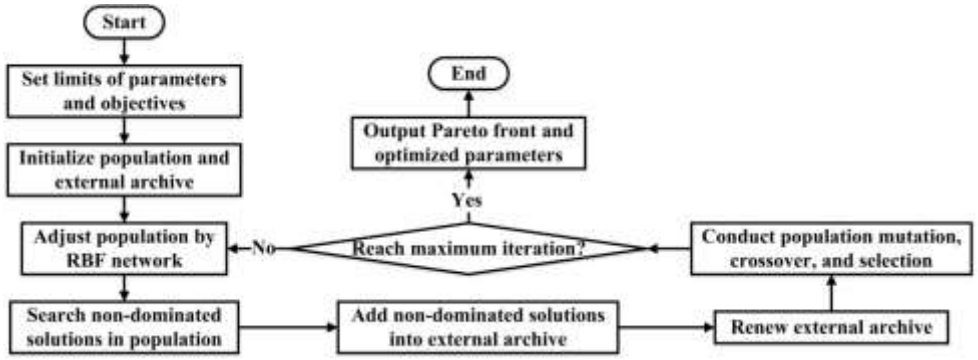

Fig. 13. Flow chart of the external archive DE algorithm.

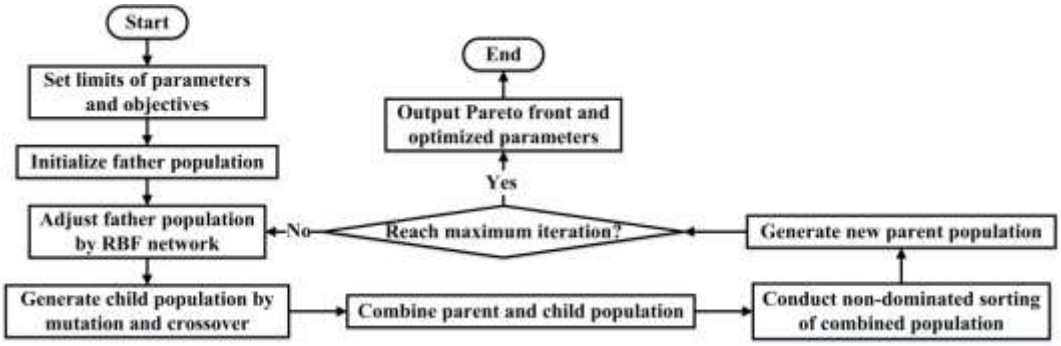

Fig. 14. Flow chart of the non-dominated sorting DE algorithm.

Besides, to accelerate the convergence of the EADE and NSDE algorithms, the upper limit of each vibration mitigation index (the original LO amplitude, mechanical energy, and input energy) is set, and the radial basis function (RBF) network is introduced. The RBF network is a very effective parameter identification method and composed of an input layer, a hidden layer, and an output layer. The characteristics and training process of the RBF network can be referred to Ref. [45]. In the training process of the current population, the variables of the input layer are the mass ratio ε and the target amplitude A, and the variables of the output layer are the three parameters of the LVA or the four parameters of the NES. As the training process is completed, the mass ratio and the target amplitude of the current population are firstly adjusted and then set as the input layer, and the adjusted parameter values of the absorber are calculated by the trained RBF network. The adjustment strategy of the mass ratio ε^* and the target amplitude A^* is

$$\varepsilon^*(i,j) = n_1 \varepsilon(i,j), A^*(i,j) = n_2 A(i,j), 1 \le i \le M,\ j \ge 0, \tag{14}$$

where n_1 and n_2 are the random numbers uniformly distributed in the interval of (0.9,1). Since there may be some deviations in the results of the RBF network, the adjusted parameter values of the absorber are returned to the dynamic equation (3) or (4) to obtain the real adjusted objective values. If the adjusted member is thoroughly superior to the original member, then the original member will be replaced by the adjusted member. If both the adjusted and original members are non-dominated solutions, and all the objective values of the adjusted member are less than their upper limit values, then a random one of these two members will be kept in the current population.

Like the single-objective DE algorithm, the population size M and the maximum iteration $j_{\max}$ also need to be fixed in the EADE and NSDE algorithms. For the population size M, too small M and too large M may not be conducive to the convergence and the diversity of the non-dominated solutions, respectively. After several trials, the proper value of M is set as 20. In the following part, the proper value of $j_{\max}$ will be sought for the convergence of the non-dominated solutions.

6 Numerical examples of multi-objective optimization

6.1 Results of the Pareto fronts

In this subsection, the results of the Pareto fronts will be used to judge the convergence of the EADE and NSDE algorithms and compare the vibration mitigation effects in the NES and the LVA and different mass ratio ε and excitation strength f_0 conditions. The results on the three objective planes that reflect the trend of the vibration mitigation effects (decay rates) changing with the mass ratio ε will be presented as the Pareto fronts of the four-objective optimization problem.

Fig. 15 shows the Pareto front of the LO-NES system in the single-frequency excitation condition (ω=1). It can be seen that the variation trends of the three decay rates are very close. In Fig. 15(a), (b), and (c), the vibration of the LO can be nearly 100% suppressed when the mass ratio of the NES is larger than 1.5% (the right side of the vertical dashed line), while the vibration mitigation effect is greatly reduced as the mass ratio is smaller than 1.5% (the left side of the vertical dashed line). In Fig. 15(d), (e), and (f), the global control effect has a positive linear relation with the mass ratio (the oblique dashed line). Besides, Fig. 15 also compares the results of the EADE and NSDE algorithms in different maximum iteration $j_{\max}$. The appropriate values of $j_{\max}$, the effectiveness of the two algorithms, and the higher computational efficiency of the NSDE algorithm are discovered. In the following calculation of sweep-frequency excitation condition, the NSDE algorithm will be adopted, and $j_{\max}$ will be set as 200.

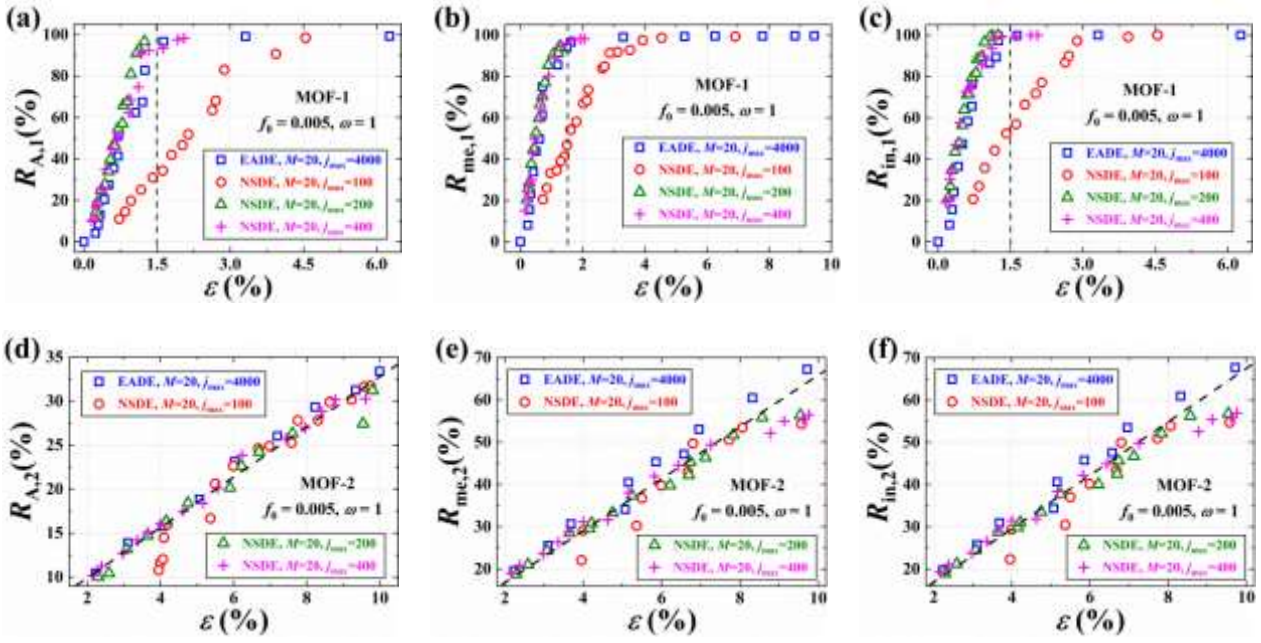

Fig. 15. Pareto fronts of the LO-NES system obtained by the EADE and NSDE algorithms in single-frequency excitation condition (f_0=0.005, ω=1): (a) the ε-$R_{A,1}$ plane in the MOF-1; (b) the ε-$R_{me,1}$ plane in the MOF-1; (c) the ε-$R_{in,1}$ plane in the MOF-1; (d) the ε-$R_{A,2}$ plane in the MOF-2; (e) the ε-$R_{me,2}$ plane in the MOF-2; (f) the ε-$R_{in,2}$ plane in the MOF-2.

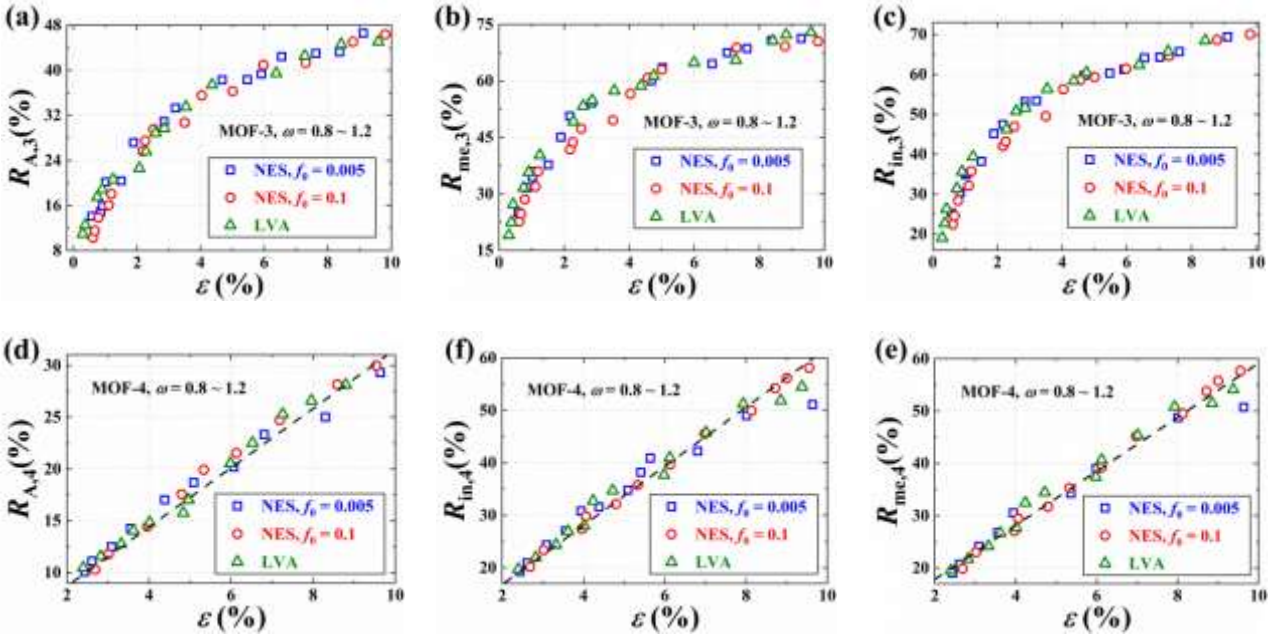

Fig. 16. Pareto fronts of the LO-LVA and LO-NES systems obtained by the NSDE algorithm in sweep-frequency excitation condition (f_0=0.005 or 0.1, ω=0.8~1.2): (a) the ε-$R_{A,3}$ plane in the MOF-3; (b) the ε-$R_{me,3}$ plane in the MOF-3; (c) the ε-$R_{in,3}$ plane in the MOF-3; (d) the ε-$R_{A,4}$ plane in the MOF-4; (e) the ε-$R_{me,4}$ plane in the MOF-4; (f) the ε-$R_{in,4}$ plane in the MOF-4.

Fig. 16 shows the Pareto fronts of the LO-LVA and LO-NES systems in the sweep-frequency excitation condition. It can be seen that the excitation strength f_0 has little effect on the variation trends of the three decay rates, which is consistent with the single-objective optimization results in

Subsection 4.2. Besides, Corresponding to Fig. 15(d), (e), and (f), the positive linear relation between the global control effect and the mass ratio can also be witnessed in Fig. 16(d), (e), and (f). In brief, the results of the Pareto fronts in Fig. 15 and Fig. 16 will help to find the solutions satisfying the actual requirements of the mass ratio and vibration mitigation.

6.2 Results of the optimized parameters of the absorbers

Subsection 6.1 presents the optimization results in the target space. However, the design of the absorbers also depends on the optimization results in the parameter space. This subsection will focus on the optimized parameters of the LVA and the NES obtained by the NSDE algorithm. Since the optimal vibration mitigation of the LO in the single-frequency excitation condition (MOF-1) requires undamped absorbers and is hard to achieve in practice, this subsection will just show the optimized parameters in the MOF-2, MOF-3, and MOF-4.

Fig. 17 shows the variation trends of the optimized damping c_2 and the optimized spring stiffness k_s of the two absorbers. In Fig. 17(a), (b), and (c), the optimized c_2 has the same positive linear relation with the mass ratio ε (the oblique dashed line) in the LVA and the NES because of the same linear damping structure. Besides, in Fig. 17(e), similar positive linear relations between the optimized k_s and ε can be witnessed in both the LVA and the NES. However, in Fig. 17(d) and (f), there are some differences in the relationship between the optimized k_s and ε in the global control of the LO-LVA and LO-NES systems. This will be explained by combining the optimization results of the geometry parameter l_1 of the NES in Table 8, where $l_{1,max}$, $l_{1,min}$, $l_{1,mean}$, and $l_{1,std}$ denote the maximum, minimum, mean value, and standard deviation of the optimized l_1 in different ε. The results in Table 8 show that the optimization values of l_1 have little change in different ε. The control of the LO is achieved by the NVA with strong positive linear stiffness ($l_1>1$), while the control of the whole system is achieved by the NES close to the monostable state ($l_1\approx1$), i.e. the bistable shallow-well NES and the NVA with weak positive linear stiffness. Since the bistable deep-well NES and the monostable NES do not have optimal vibration mitigation effects in certain excitation conditions of single-objective optimization, they are also absent from the multi-objective optimization. As the single-objective optimization results in Table 3, Table 5, and Fig. 6 show that the NES close to the monostable state will possess large optimal values of k_s, this feature will also be reflected in the multi-objective design of k_s. Furthermore, the results in Fig. 17(d) and (f) indicate the decrease of the optimized k_s of the NES close to the monostable state when the excitation strength f_0 increases.

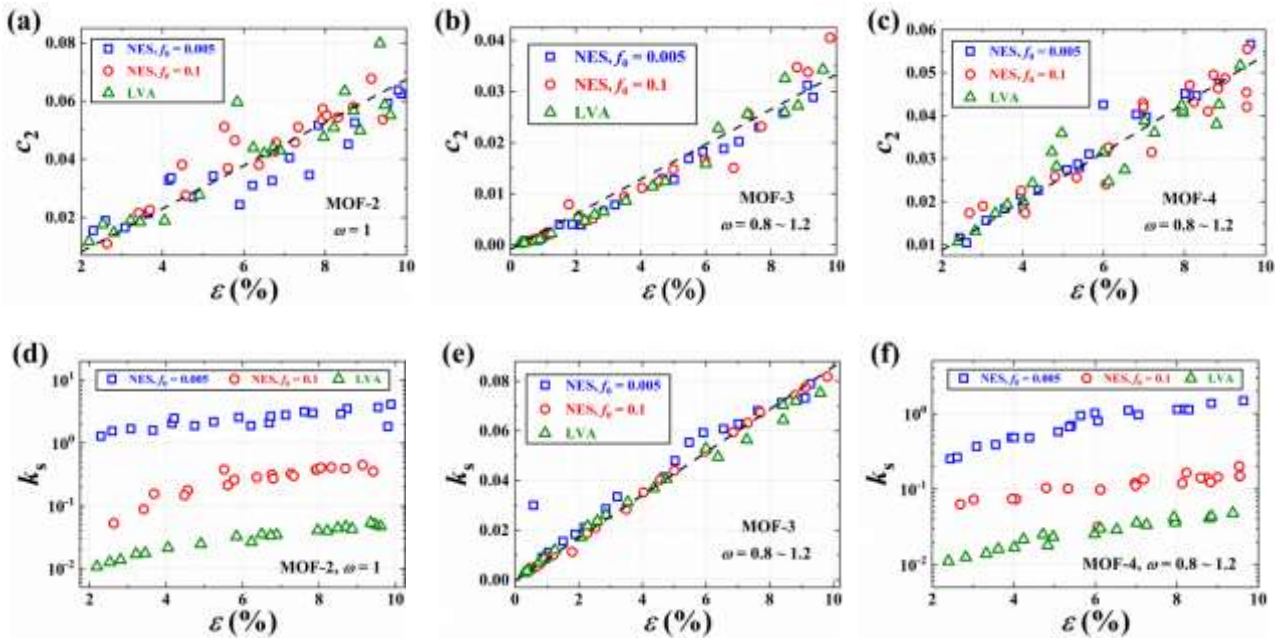

Fig. 17. Trends of the optimized damping c_2 and the optimized spring stiffness k_s changing with the mass ratio ε obtained by the NSDE algorithm in different MOFs and excitation conditions (f_0=0.005 or 0.1): (a) and (d) MOF-2; (b) and (e) MOF-3; (c) and (f) MOF-4.

Table 8 Statistical results of the optimized geometry parameter l_1 in different MOFs and excitation conditions.

Objective function	f_0	$l_{1,max}$	$l_{1,min}$	$l_{1,mean}$	$l_{1,std}$
MOFs-2	0.005	0.9973	0.9934	0.9962	0.0009
MOFs-2	0.1	1.0260	0.9571	0.9921	0.0167
MOFs-3	0.005	1.9436	1.0957	1.7942	0.1833
MOFs-3	0.1	1.8310	1.5023	1.7239	0.1072
MOFs-4	0.005	1.0233	0.9906	1.0106	0.0124
MOFs-4	0.1	1.1700	1.0076	1.0832	0.0562

From the above analysis, the multi-objective and multi-parameter design procedure of the LVA and the NES can be summarized:

(i) Determine the target of vibration mitigation, such as the vibration control of the main system or the whole system.

(ii) Determine the appropriate range of the geometry parameter l_1 in the bistable shallow-well NES and the NVA with positive linear stiffness.

(iii) Find the appropriate range of the mass ratio ε by the Pareto fronts and the actual demand.

(iv) For the LVA, the optimal ranges of the damping c_2 and the spring stiffness k_s will be fixed by the positive linear relations with ε.

(v) For the NES, the optimal range of c_2 is the same as that of the LVA, while the optimal range of k_s will be adjusted by l_1 and excitation strength f_0. The closer the NES is to the monostable state or the smaller f_0 is, the larger k_s is.

7 Conclusions

This paper proposes a new vibration control strategy in harmonic excitation, namely the global control of the linear main system coupled with the absorber by using the differential evolutionary (DE) algorithm. Compared with the large amplitude of the absorber and the variation of the resonance frequency in the local control of the main system, the global control can diminish the maximum amplitudes of both the main system and the absorber and maintain the resonance frequency of the main system. So the global control strategy has high application value.

This paper also compares the similarities and disparities between the linear vibration absorber (LVA) and the nonlinear energy sink (NES) in vibration mitigation and parameter design in single- and multi-objective optimization. In the single-objective optimization, the optimal LVA and the optimal NES have almost the same vibration mitigation effects, mass ratio, damping, and frequency responses in small excitation. Different from the LVA, the NES has multiple optimal combinations of spring stiffness and geometry parameter; the NES can achieve decent vibration mitigation effects in a wider range of spring stiffness, where the monostable NES and the bistable NES have the best stiffness robustness in small and large excitation conditions, respectively; the optimal NES has better frequency response than the optimal LVA in large excitation.

In the multi-objective optimization, mass ratio, displacement amplitude, mechanical energy, and input energy are taken as objectives, and the Pareto fronts and optimized parameters of the LVA and the NES are obtained by the multi-objective DE algorithms. Based on these results, multi-objective and multi-parameter design criteria for the LVA and the NES are presented. The main points are as follows: The NES should be designed as the bistable one close to the monostable state or the nonlinear vibration absorber with positive linear stiffness. The mass ratio and damping of the NES can be determined by the LVA. The spring stiffness of the NES should be determined by the geometry parameter and excitation strength. Especially, the bistable NES close to the monostable state requires a higher spring stiffness value than the LVA.

The global control strategy proposed in this paper is implemented in a single-degree-of-freedom main system. If this strategy is applied to the multi-degree-of-freedom main system, the vibration mitigation effect and the influence on the resonance frequency need further investigation. Besides, the linear damping structure of the absorbers has great impacts on vibration mitigation. In future work, the damping structure of the absorbers will be improved for higher damping robustness.

Acknowledgments

The authors gratefully acknowledge the support of the National Natural Science Foundation of China (No. 12025204) and the Program of Shanghai Municipal Education Commission (No. 2019-01-07-00-09-E00018).

Conflicts of interest: The authors declare that they have no conflict of interest.

Data availability statements: The data that support the findings of this study are available from the corresponding author, [H. Ding], upon reasonable request.

References

1. Concha, A., Thenozhi, S., Betancourt, R.J., Gadi, S.K.: A tuning algorithm for a sliding mode controller of buildings with ATMD. Mech. Syst. Signal Process. 154, 107539 (2021). doi:10.1016/j.ymssp.2020.107539
2. da Costa, M.M.A., Castello, D.A., Magluta, C., Roitman, N.: On the optimal design and robustness of spatially distributed tuned mass dampers. Mech. Syst. Signal Process. 150, 107289 (2021). doi:10.1016/j.ymssp.2020.107289
3. Ebrahimzade, N., Dardel, M., Shafaghat, R.: Performance comparison of linear and nonlinear vibration absorbers in aeroelastic characteristics of a wing model. Nonlinear Dyn. 86, 1075–1094 (2016). doi:10.1007/s11071-016-2948-1
4. Vakakis, A.F., Gendelman, O.: Energy pumping in nonlinear mechanical oscillators: Part II—Resonance capture. J. Appl. Mech. 68, 42–48 (2001). doi:10.1115/1.1345525
5. Chen, H.Y., Mao, X.Y., Ding, H., Chen, L.Q.: Elimination of multimode resonances of composite plate by inertial nonlinear energy sinks. Mech. Syst. Signal Process. 135, 106383 (2020). doi:10.1016/j.ymssp.2019.106383
6. Bergeot, B., Bellizzi, S., Berger, S.: Dynamic behavior analysis of a mechanical system with two unstable modes coupled to a single nonlinear energy sink. Commun. Nonlinear Sci. Numer. Simul. 95, 105623 (2021). doi:10.1016/j.cnsns.2020.105623
7. Khazaee, M., Khadem, S.E., Moslemi, A., Abdollahi, A.: Vibration mitigation of a pipe conveying fluid with a passive geometrically nonlinear absorber: a tuning optimal design. Commun. Nonlinear Sci. Numer. Simul. 91, 105439 (2020). doi:10.1016/j.cnsns.2020.105439
8. Tehrani, G.G., Dardel, M.: Vibration mitigation of a flexible bladed rotor dynamic system with passive dynamic absorbers. Commun. Nonlinear Sci. Numer. Simul. 69, 1–30 (2019).

doi:10.1016/j.cnsns.2018.08.007

9. Gomez, F., Fermandois, G.A., Spencer, B.F.: Optimal design of nonlinear energy sinks for mitigation of seismic response on structural systems. Eng. Struct. 232, 111756 (2021). doi:10.1016/j.engstruct.2020.111756
10. Habib, G., Kerschen, G.: A principle of similarity for nonlinear vibration absorbers. Phys. D Nonlinear Phenom. 332, 1–8 (2016). doi:10.1016/j.physd.2016.06.001
11. Habib, G., Romeo, F.: The tuned bistable nonlinear energy sink. Nonlinear Dyn. 89, 179–196 (2017). doi:10.1007/s11071-017-3444-y
12. Benacchio, S., Malher, A., Boisson, J., Touzé, C.: Design of a magnetic vibration absorber with tunable stiffnesses. Nonlinear Dyn. 85, 893–911 (2016). doi:10.1007/s11071-016-2731-3
13. Farid, M., Gendelman, O. V.: Tuned pendulum as nonlinear energy sink for broad energy range. J. Vib. Control. 23, 373–388 (2017). doi:10.1177/1077546315578561
14. Farid, M., Gendelman, O. V., Babitsky, V.I.: Dynamics of a hybrid vibro-impact nonlinear energy sink. ZAMM - J. Appl. Math. Mech. / Zeitschrift für Angew. Math. und Mech. e201800341 (2019). doi:10.1002/zamm.201800341
15. Taghipour, J., Dardel, M., Pashaei, M.H.: Vibration mitigation of a nonlinear rotor system with linear and nonlinear vibration absorbers. Mech. Mach. Theory. 128, 586–615 (2018). doi:10.1016/j.mechmachtheory.2018.07.001
16. Wang, J.J., Wang, B., Liu, Z. Bin, Li, H.B., Zhang, C.: Seismic response mitigation of building structures with a novel vibro-impact dual-mass damper. Eng. Struct. 215, 110673 (2020). doi:10.1016/j.engstruct.2020.110673
17. Wang, G.X., Ding, H., Chen, L.Q.: Nonlinear normal modes and optimization of a square root nonlinear energy sink. Nonlinear Dyn. (2021). doi:10.1007/s11071-021-06334-1
18. Zhang, P., Li, L., Patil, D., Singla, M., Li, H.N., Mo, Y.L., Song, G.: Parametric study of pounding tuned mass damper for subsea jumpers. Smart Mater. Struct. 25, 015028 (2016). doi:10.1088/0964-1726/25/1/015028
19. Geng, X.F., Ding, H., Wei, K.X., Chen, L.Q.: Suppression of multiple modal resonances of a cantilever beam by an impact damper. Appl. Math. Mech. Ed. 41, 383–400 (2020). doi:10.1007/s10483-020-2588-9
20. Fang, B., Theurich, T., Krack, M., Bergman, L.A., Vakakis, A.F.: Vibration suppression and modal energy transfers in a linear beam with attached vibro-impact nonlinear energy sinks. Commun. Nonlinear Sci. Numer. Simul. 91, 105415 (2020). doi:10.1016/j.cnsns.2020.105415
21. Geng, X.F., Ding, H., Mao, X.Y., Chen, L.Q.: Nonlinear energy sink with limited vibration amplitude. Mech. Syst. Signal Process. 156, 107625 (2021).

doi:10.1016/j.ymssp.2021.107625

22. Romeo, F., Sigalov, G., Bergman, L.A., Vakakis, A.F.: Dynamics of a linear oscillator coupled to a bistable light attachment: numerical study. J. Comput. Nonlinear Dyn. 10, 011007 (2015). doi:10.1115/1.4027224
23. Dekemele, K., Keyser, R. De, Loccufier, M.: Performance measures for targeted energy transfer and resonance capture cascading in nonlinear energy sinks. Nonlinear Dyn. 93, 259–284 (2018). doi:10.1007/s11071-018-4190-5
24. Dekemele, K., Van Torre, P., Loccufier, M.: Performance and tuning of a chaotic bi-stable NES to mitigate transient vibrations. Nonlinear Dyn. 98, 1831–1851 (2019). doi:10.1007/s11071-019-05291-0
25. Dekemele, K., Van Torre, P., Loccufier, M.: Design, construction and experimental performance of a nonlinear energy sink in mitigating multi-modal vibrations. J. Sound Vib. 473, 115243 (2020). doi:10.1016/j.jsv.2020.115243
26. Qiu, D., Li, T., Seguy, S., Paredes, M.: Efficient targeted energy transfer of bistable nonlinear energy sink: application to optimal design. Nonlinear Dyn. 92, 443–461 (2018). doi:10.1007/s11071-018-4067-7
27. Yang, K., Zhang, Y.W., Ding, H., Chen, L.Q.: The transmissibility of nonlinear energy sink based on nonlinear output frequency-response functions. Commun. Nonlinear Sci. Numer. Simul. 44, 184–192 (2017). doi:10.1016/j.cnsns.2016.08.008
28. Zang, J., Zhang, Y.W., Ding, H., Yang, T.Z., Chen, L.Q.: The evaluation of a nonlinear energy sink absorber based on the transmissibility. Mech. Syst. Signal Process. 125, 99–122 (2019). doi:10.1016/j.ymssp.2018.05.061
29. Huang, D.M., Li, R.H., Yang, G.D.: On the dynamic response regimes of a viscoelastic isolation system integrated with a nonlinear energy sink. Commun. Nonlinear Sci. Numer. Simul. 79, 104916 (2019). doi:10.1016/j.cnsns.2019.104916
30. Wang, J.J., Wierschem, N.E., Wang, B., Spencer, B.F.: Multi-objective design and performance investigation of a high-rise building with track nonlinear energy sinks. Struct. Des. Tall Spec. Build. 29, e1692 (2020). doi:10.1002/tal.1692
31. Qiu, D., Seguy, S., Paredes, M.: Design criteria for optimally tuned vibro-impact nonlinear energy sink. J. Sound Vib. 442, 497–513 (2019). doi:10.1016/j.jsv.2018.11.021
32. Li, W.K., Wierschem, N.E., Li, X.H., Yang, T.J., Brennan, M.J.: Numerical study of a symmetric single-sided vibro-impact nonlinear energy sink for rapid response reduction of a cantilever beam. Nonlinear Dyn. 100, 951–971 (2020). doi:10.1007/s11071-020-05571-0
33. Li, H.Q., Li, A., Kong, X.R.: Design criteria of bistable nonlinear energy sink in steady-state dynamics of beams and plates. Nonlinear Dyn. 103, 1475–1497 (2021). doi:10.1007/s11071-020-06178-1

34. Raj, P.V.R., Santhosh, B.: Parametric study and optimization of linear and nonlinear vibration absorbers combined with piezoelectric energy harvester. Int. J. Mech. Sci. 152, 268–279 (2019). doi:10.1016/j.ijmecsci.2018.12.053
35. Khazaee, M., Khadem, S.E., Moslemi, A., Abdollahi, A.: A comparative study on optimization of multiple essentially nonlinear isolators attached to a pipe conveying fluid. Mech. Syst. Signal Process. 141, 106442 (2020). doi:10.1016/j.ymssp.2019.106442
36. Gourdon, E., Alexander, N.A., Taylor, C.A., Lamarque, C.H., Pernot, S.: Nonlinear energy pumping under transient forcing with strongly nonlinear coupling: Theoretical and experimental results. J. Sound Vib. 300, 522–551 (2007). doi:10.1016/j.jsv.2006.06.074
37. AL-Shudeifat, M.A.: Highly efficient nonlinear energy sink. Nonlinear Dyn. 76, 1905–1920 (2014). doi:10.1007/s11071-014-1256-x
38. Chen, J.E., Sun, M., Hu, W.H., Zhang, J.H., Wei, Z.C.: Performance of non-smooth nonlinear energy sink with descending stiffness. Nonlinear Dyn. 100, 255–267 (2020). doi:10.1007/s11071-020-05528-3
39. Zang, J., Chen, L.Q.: Complex dynamics of a harmonically excited structure coupled with a nonlinear energy sink. Acta Mech. Sin. 33, 801–822 (2017). doi:10.1007/s10409-017-0671-x
40. Price, K. V., Storn, R.M., Lampinen, J.A.: Differential evolution: a practical approach to global optimization. Springer-Verlag, Berlin/Heidelberg (2005)
41. He, J., Lin, G.M.: Average convergence rate of evolutionary algorithms. IEEE Trans. Evol. Comput. 20, 316–321 (2016). doi:10.1109/TEVC.2015.2444793
42. Knobloch, R., Mlynek, J., Srb, R.: Improving convergence properties of a differential evolution algorithm. In: AIP Conference Proceedings. p. 030005 (2016)
43. Zhang, Z.H., Zhong, C.Q., Xu, Z.Z., Teng, H.F.: A non-dominated sorting cooperative co-evolutionary differential evolution algorithm for multi-objective layout optimization. IEEE Access. 5, 14468–14477 (2017). doi:10.1109/ACCESS.2017.2716111
44. Liang, Z.P., Wang, X.Y., Lin, Q.Z., Chen, F., Chen, J.Y., Ming, Z.: A novel multi-objective co-evolutionary algorithm based on decomposition approach. Appl. Soft Comput. J. 73, 50–66 (2018). doi:10.1016/j.asoc.2018.08.020
45. Liu, J.K.: Radial basis function (RBF) neural network control for mechanical systems: design, analysis and Matlab simulation. Springer Berlin Heidelberg, Berlin, Heidelberg (2013)

Figures

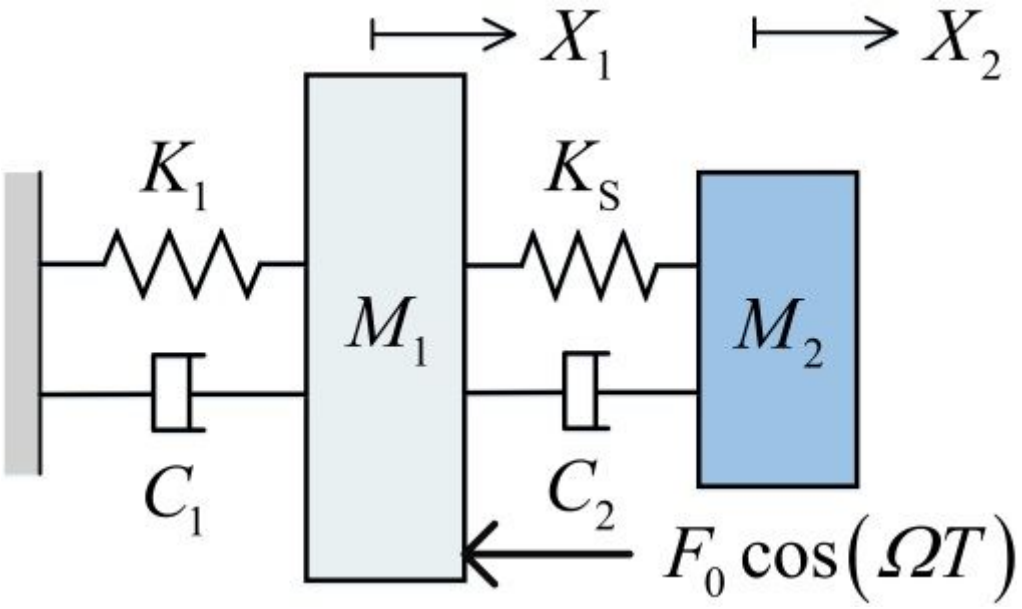

Figure 1

Model of an LO coupled with an LVA.

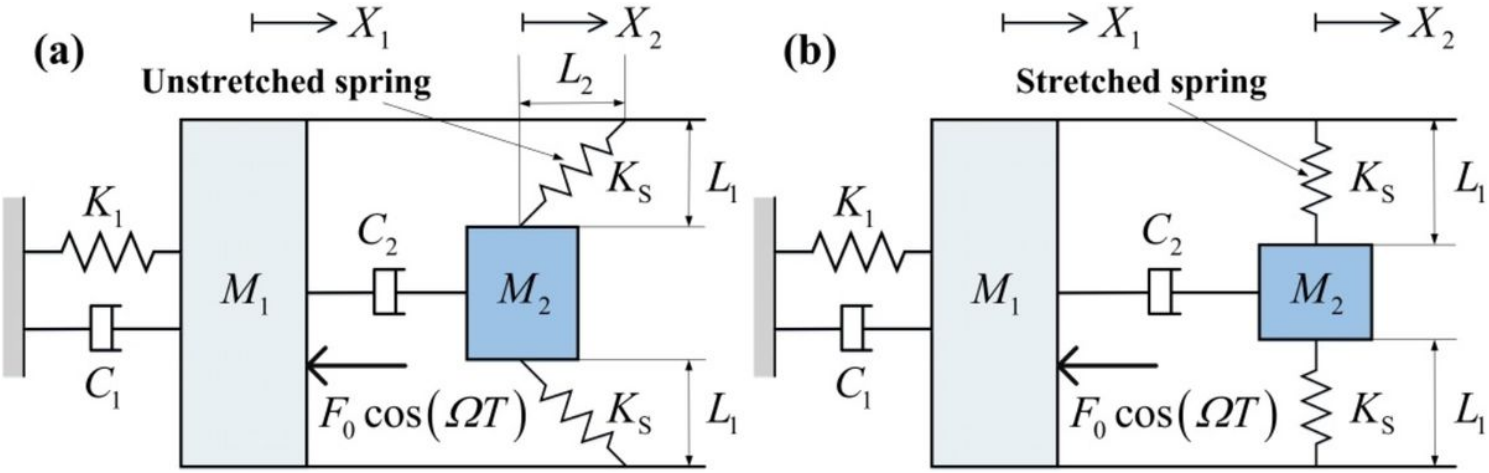

Figure 2

Model of an LO coupled with an NES: (a) L1≤L, L2≥0, L12+L22=L2; (b) L1>L, L2=0.

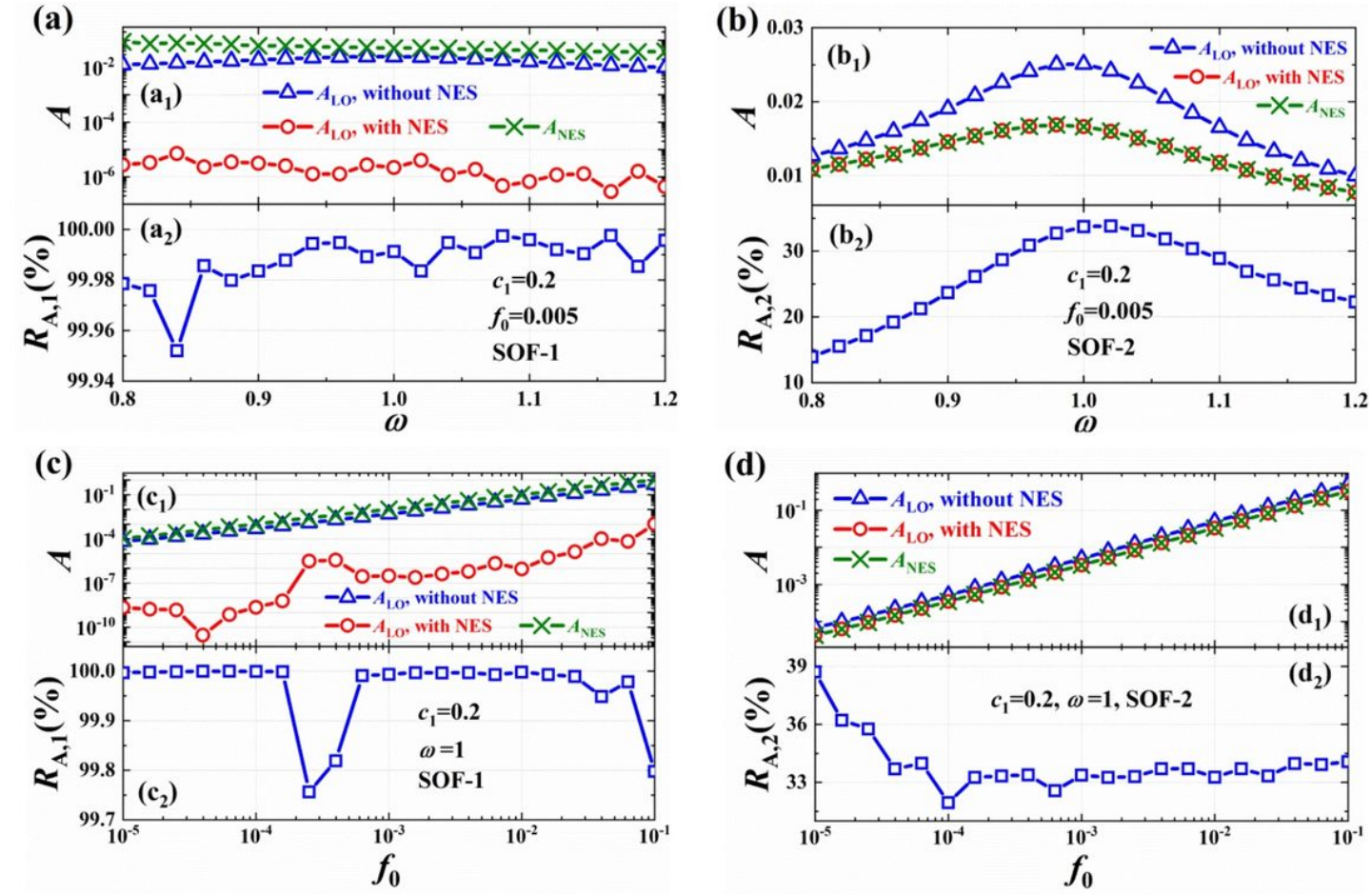

Figure 3

Amplitudes of the LO and the NES and amplitude decay rate in different objective and single-frequency excitation conditions: (a) and (b) SOF-1 & SOF-2, f0=0.005, ω=0.8~1.2; (c) and (d) SOF-1 & SOF-2, ω=1, lg(f0)=-5~-1.

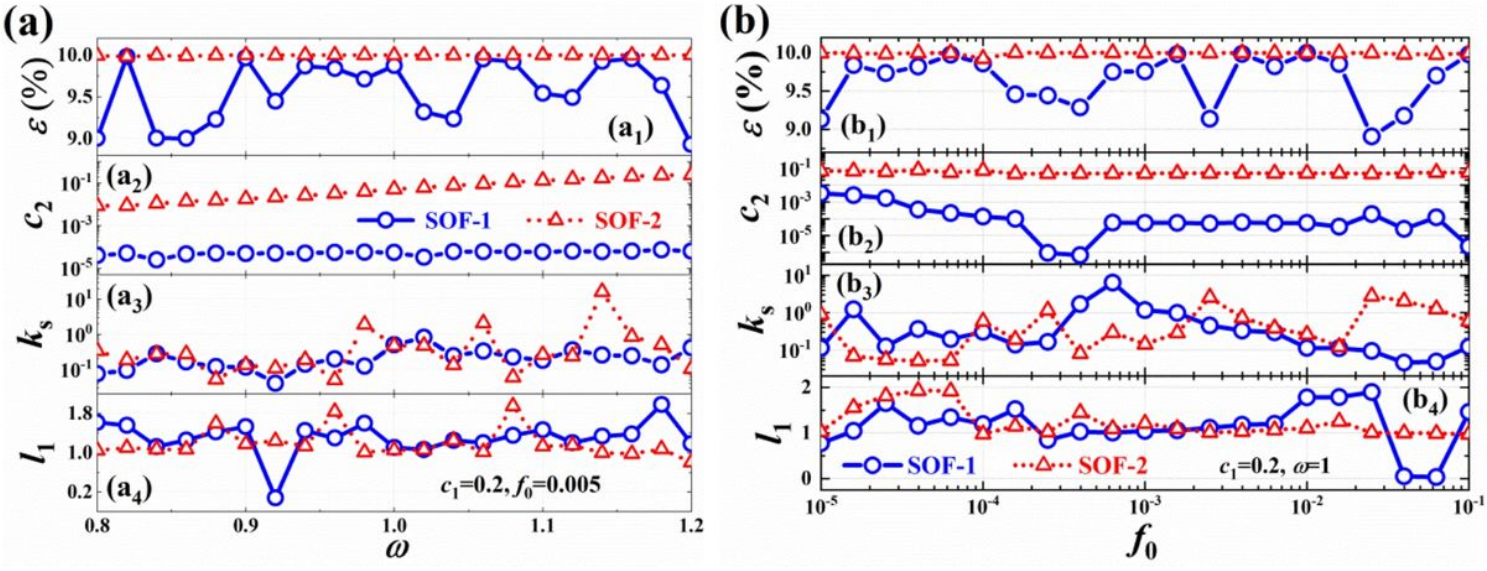

Figure 4

Optimal parameters of the NES in different objective and single-frequency excitation conditions: (a) SOF-1 & SOF-2, f0=0.005, ω=0.8~1.2; (b) SOF-1 & SOF-2, ω=1, lg(f0)=-5~-1.

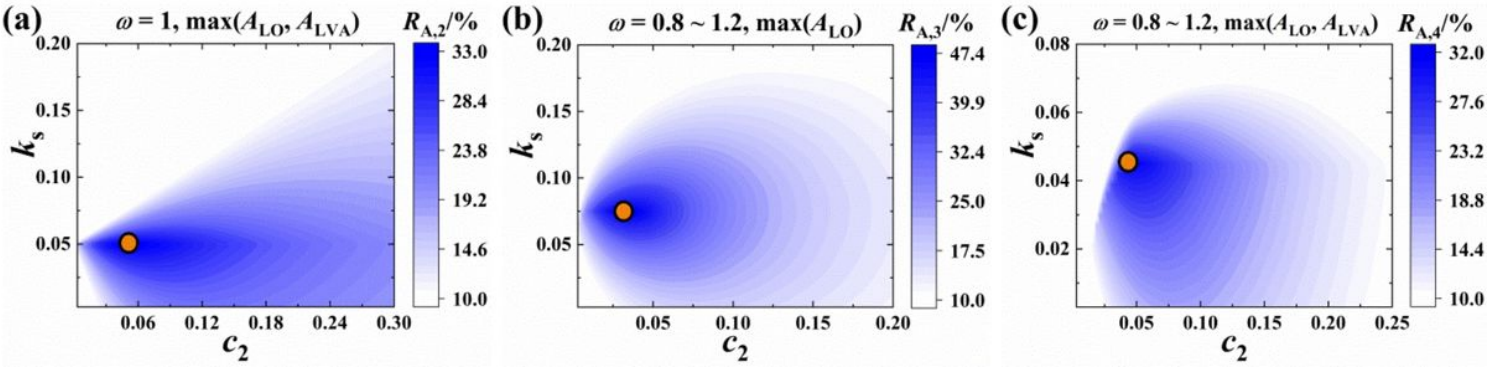

Figure 5

Amplitude decay rates of the LO-LVA system with f0=0.005 or 0.1, ε=0.1, and varied damping c2, spring stiffness ks, and SOFs, where the circles denote the results of the DE algorithm: (a) SOF-2; (b) SOF-3; (c) SOF-4.

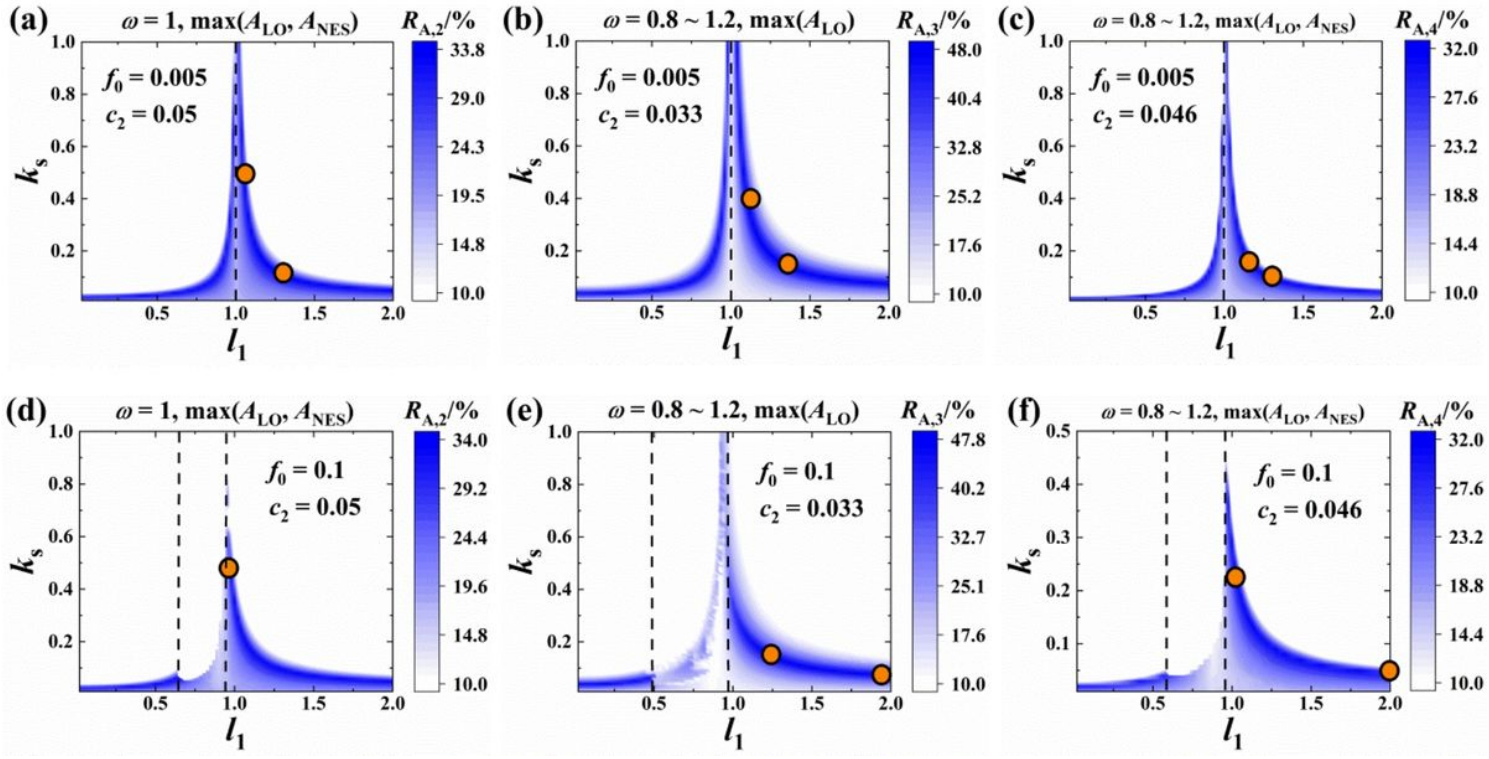

Figure 6

Amplitude decay rates of the LO-NES system with f0=0.005 or 0.1, ε=0.1, optimal damping c2, and varied spring stiffness ks, geometry parameter l1, and SOFs, where the circles denote the results of the DE algorithm: (a) and (d) SOF-2; (b) and (e) SOF-3; (c) and (f) SOF-4.

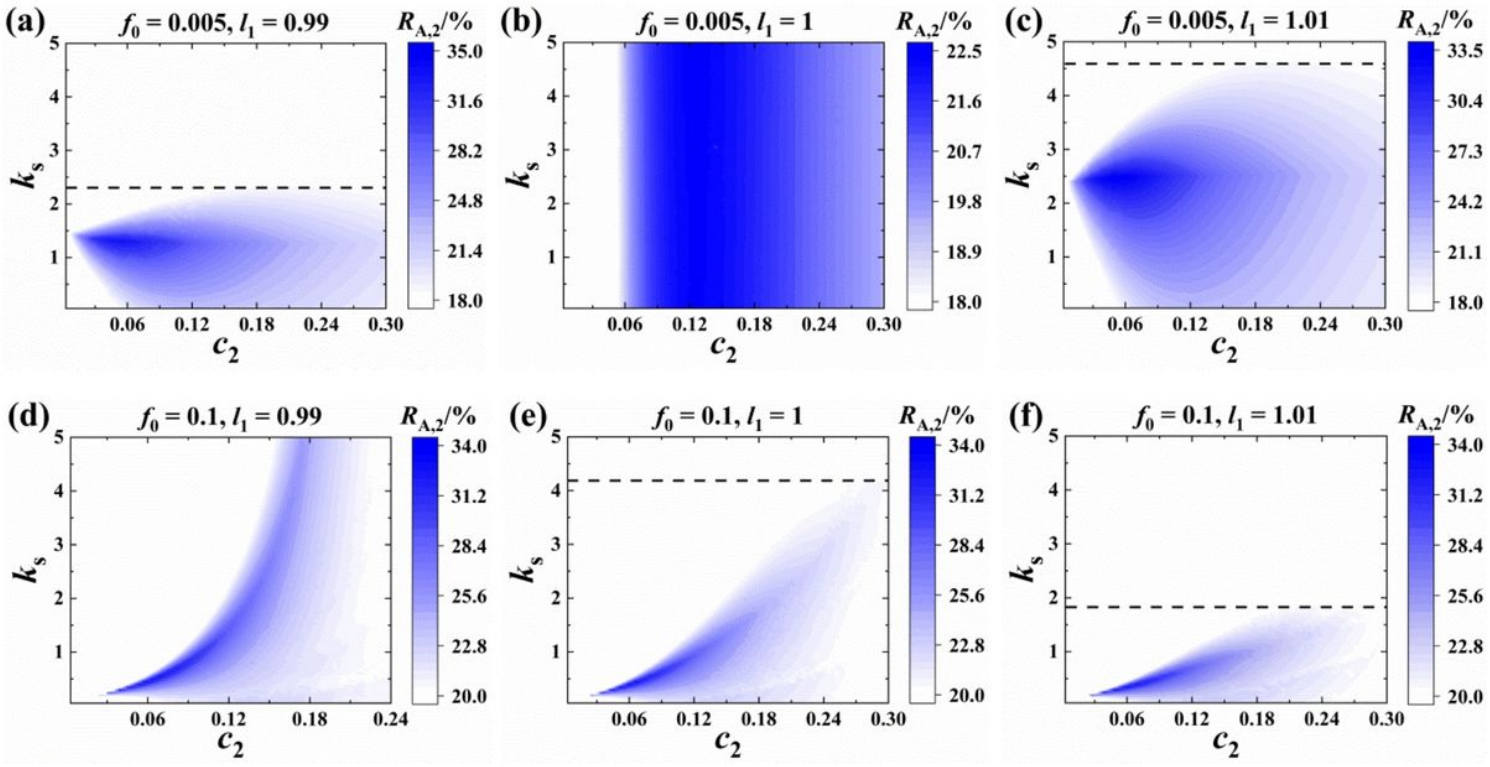

Figure 7

Amplitude decay rate RA,2 of the LO-NES system with f0=0.005 or 0.1, ε=0.1, and varied damping c2, spring stiffness ks, geometry parameter l1 in the SOF-2, where the dashed lines denote the upper limit values of effective ks: (a) and (d) the bistable NES with l1=0.99; (b) and (e) the monostable NES with l1=1; (c) and (f) the NVA with l1=1.01.

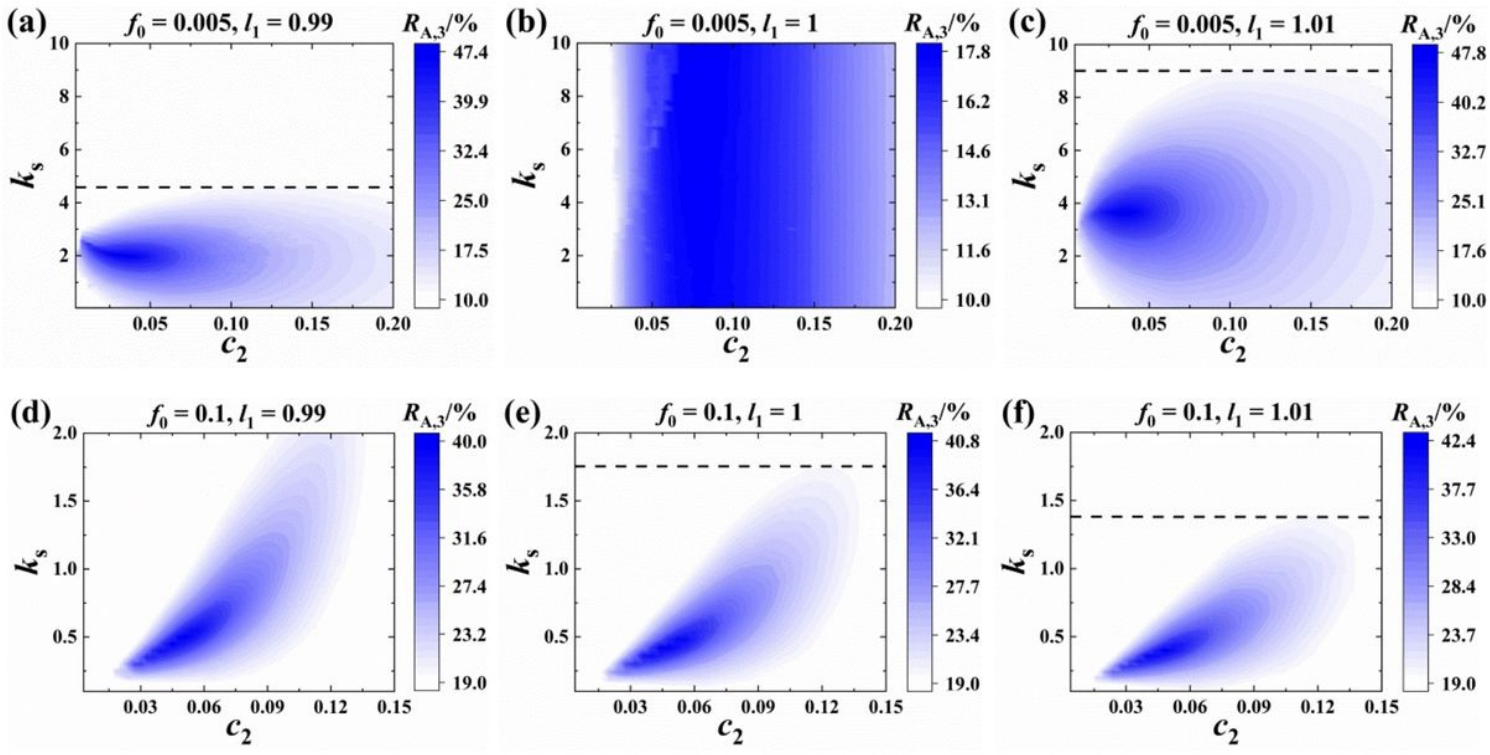

Figure 8

Amplitude decay rate RA,3 of the LO-NES system with f0=0.005 or 0.1, ε=0.1, and varied damping c2, spring stiffness ks, geometry parameter l1 in the SOF-3, where the dashed lines denote the upper limit values of effective ks: (a) and (d) the bistable NES with l1=0.99; (b) and (e) the monostable NES with l1=1; (c) and (f) the NVA with l1=1.01.

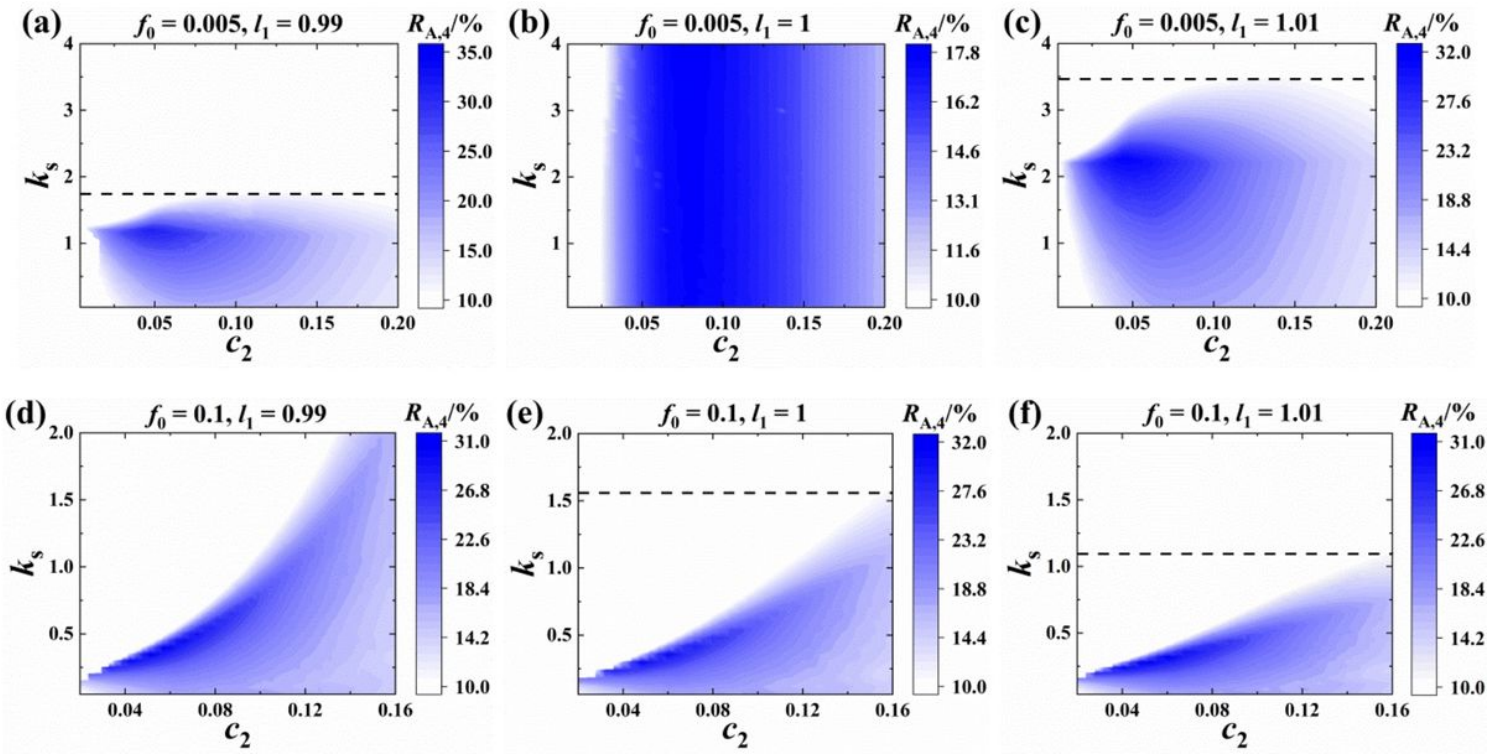

Figure 9

Amplitude decay rate RA,4 of the LO-NES system with f0=0.005 or 0.1, ε=0.1, and varied damping c2, spring stiffness ks, geometry parameter l1 in the SOF-4, where the dashed lines denote the upper limit values of effective ks: (a) and (d) the bistable NES with l1=0.99; (b) and (e) the monostable NES with l1=1; (c) and (f) the NVA with l1=1.01.

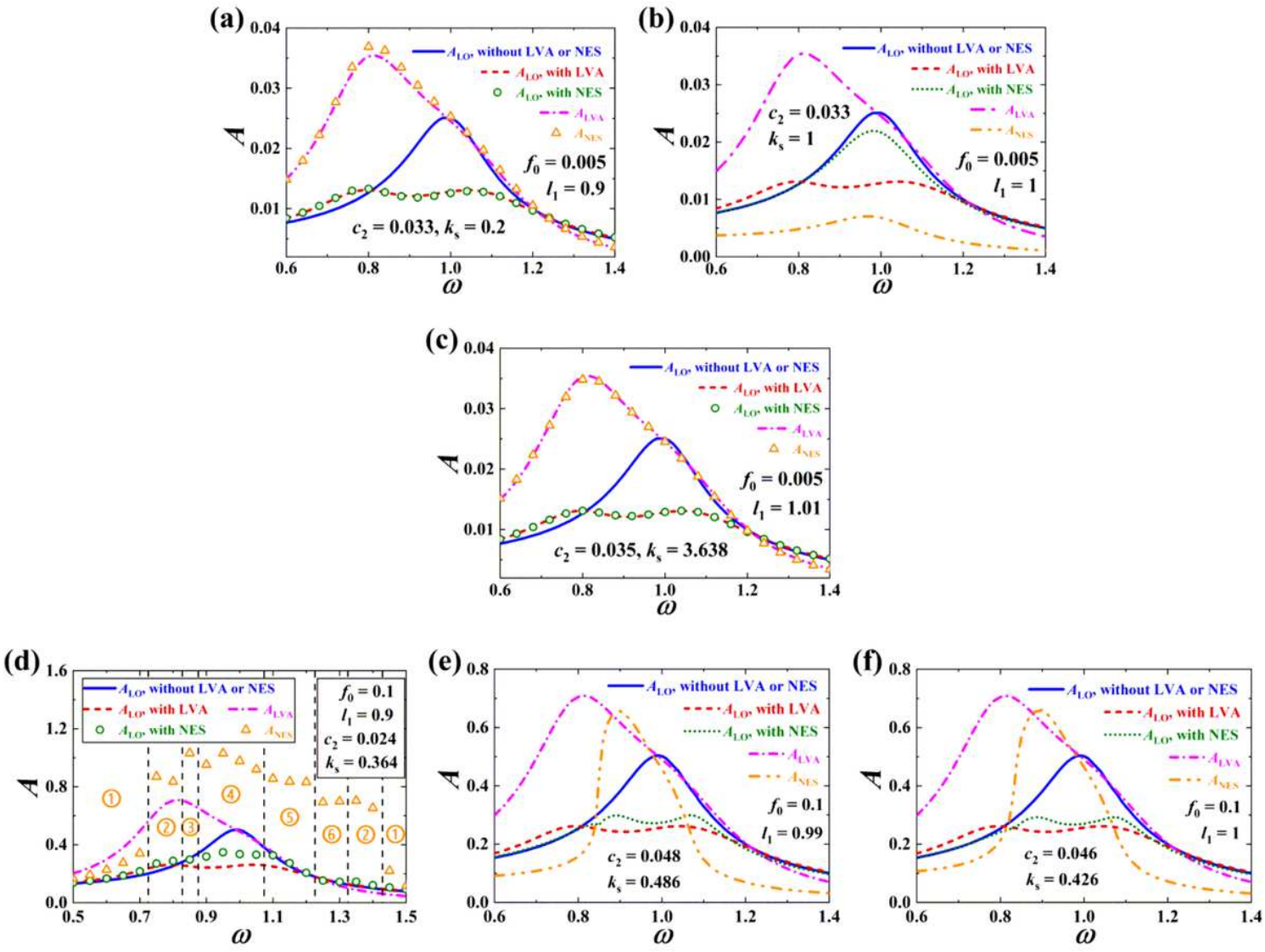

Figure 10

Frequency responses of the LO coupled with the optimal LVA or the optimal NES in different excitation and geometry conditions, ε=0.1, and the SOF-3: (a) f0=0.005, l1=0.9; (b) f0=0.005, l1=1; (c) f0=0.005, l1=1.01; (d) f0=0.1, l1=0.9; (e) f0=0.1, l1=0.99; (f) f0=0.1, l1=1.

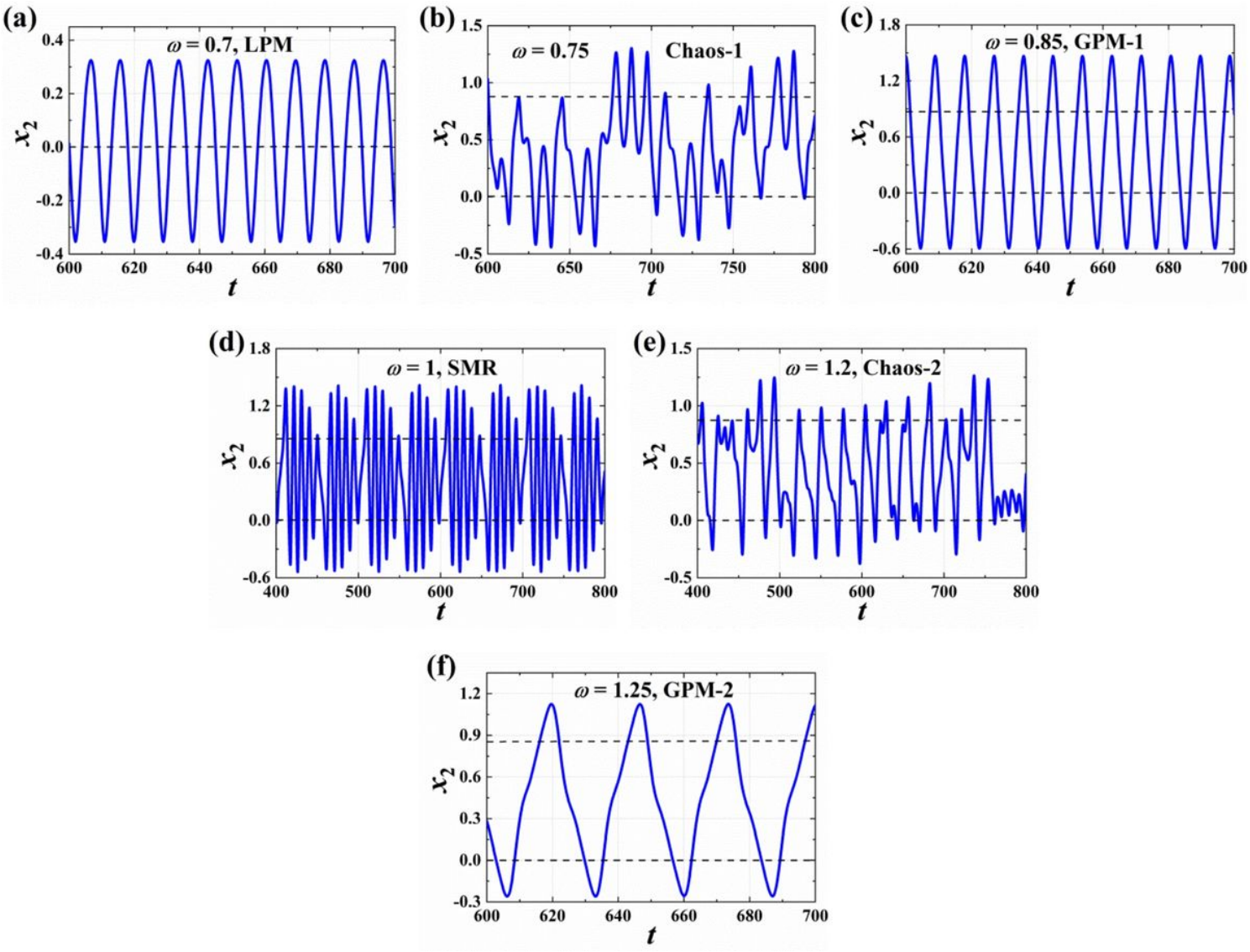

Figure 11

Displacement time histories of the bistable NES in different excitation frequency conditions in Fig. 10(d): (a) local periodic motion with ω=0.7; (b) chaos dominated by in-well motion with ω=0.75; (c) global periodic motion dominated by excitation frequency with ω=0.85; (d) strongly modulated response with ω=1; (e) chaos dominated by cross-well motion with ω=1.2; (f) global periodic motion dominated by low-frequency component with ω=1.25.

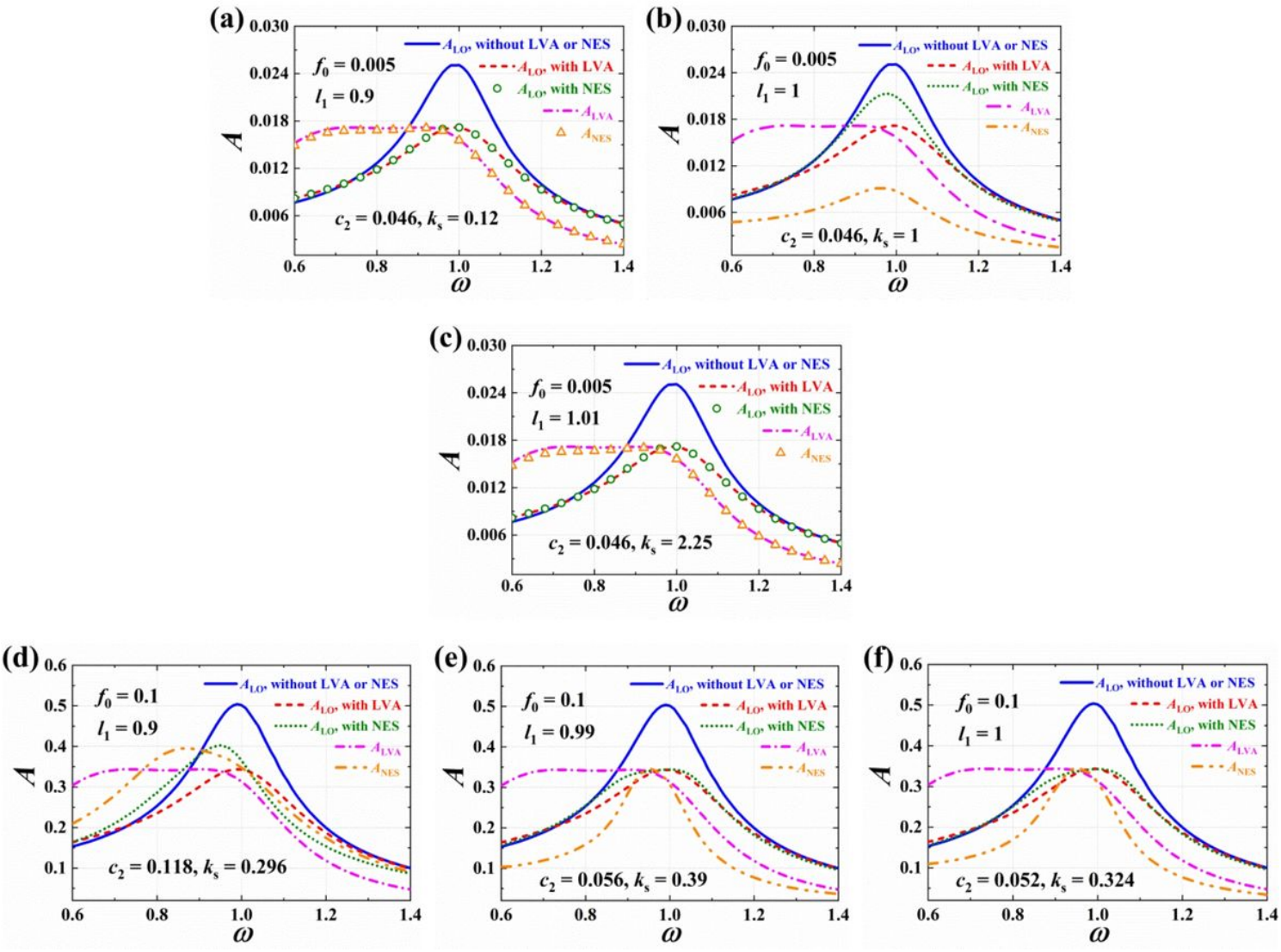

Figure 12

Frequency responses of the LO coupled with the optimal LVA or the optimal NES in different excitation and geometry conditions, ε=0.1, and the SOF-4: (a) f0=0.005, l1=0.9; (b) f0=0.005, l1=1; (c) f0=0.005, l1=1.01; (d) f0=0.1, l1=0.9; (e) f0=0.1, l1=0.99; (f) f0=0.1, l1=1.

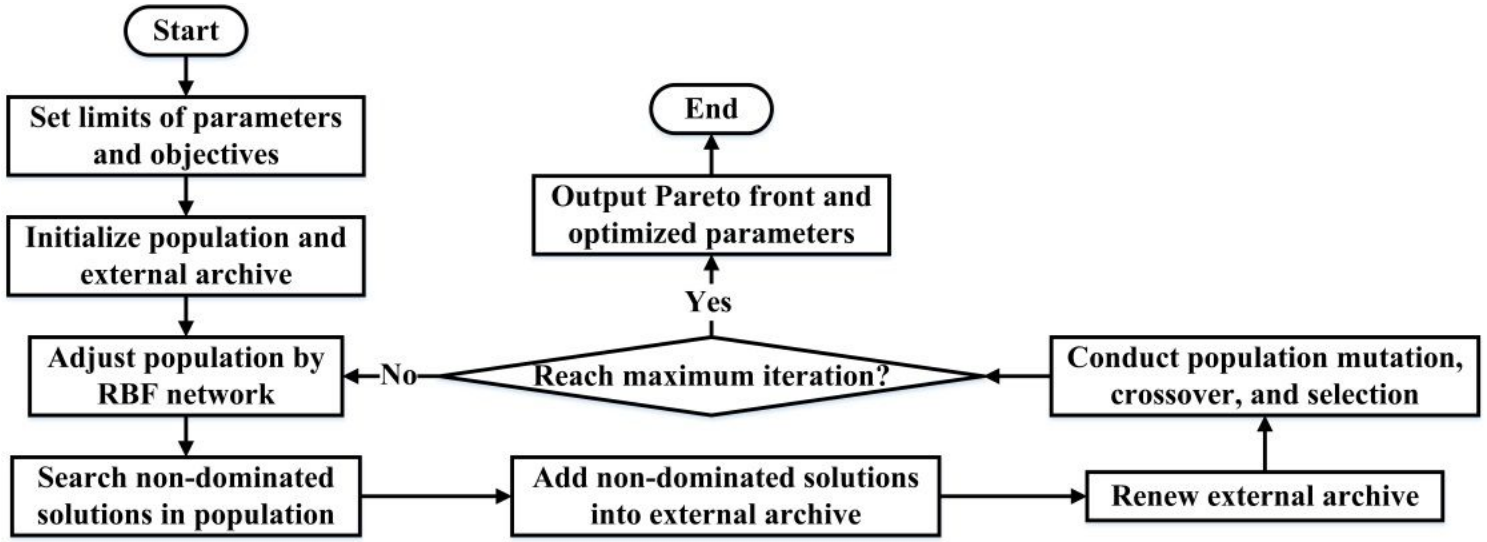

Figure 13

Flow chart of the external archive DE algorithm.

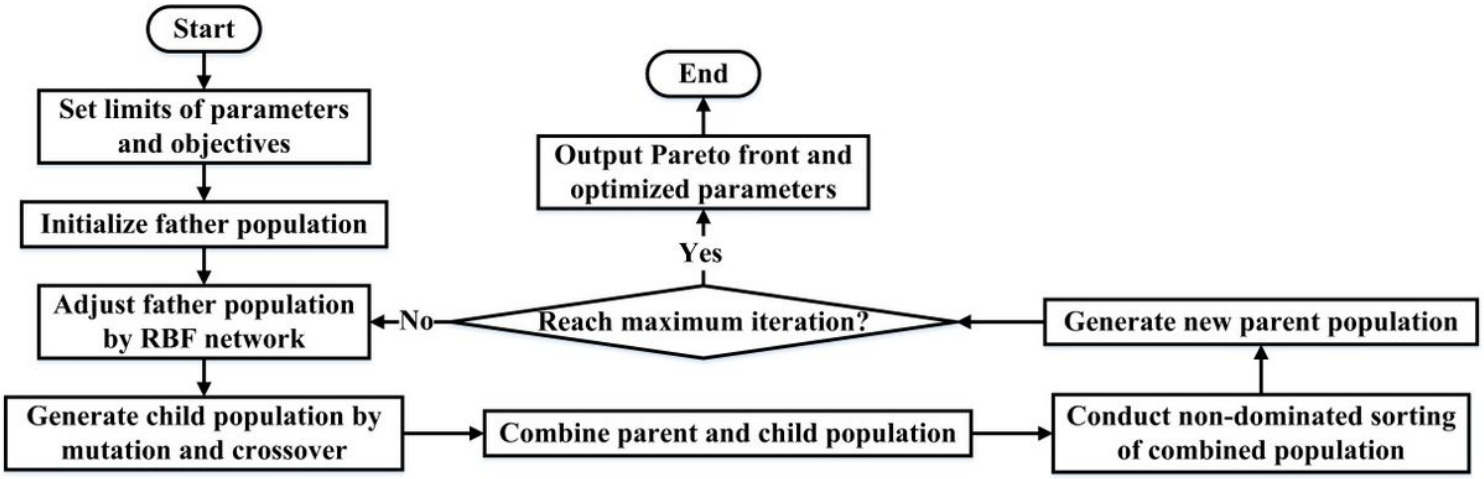

Figure 14

Flow chart of the non-dominated sorting DE algorithm.

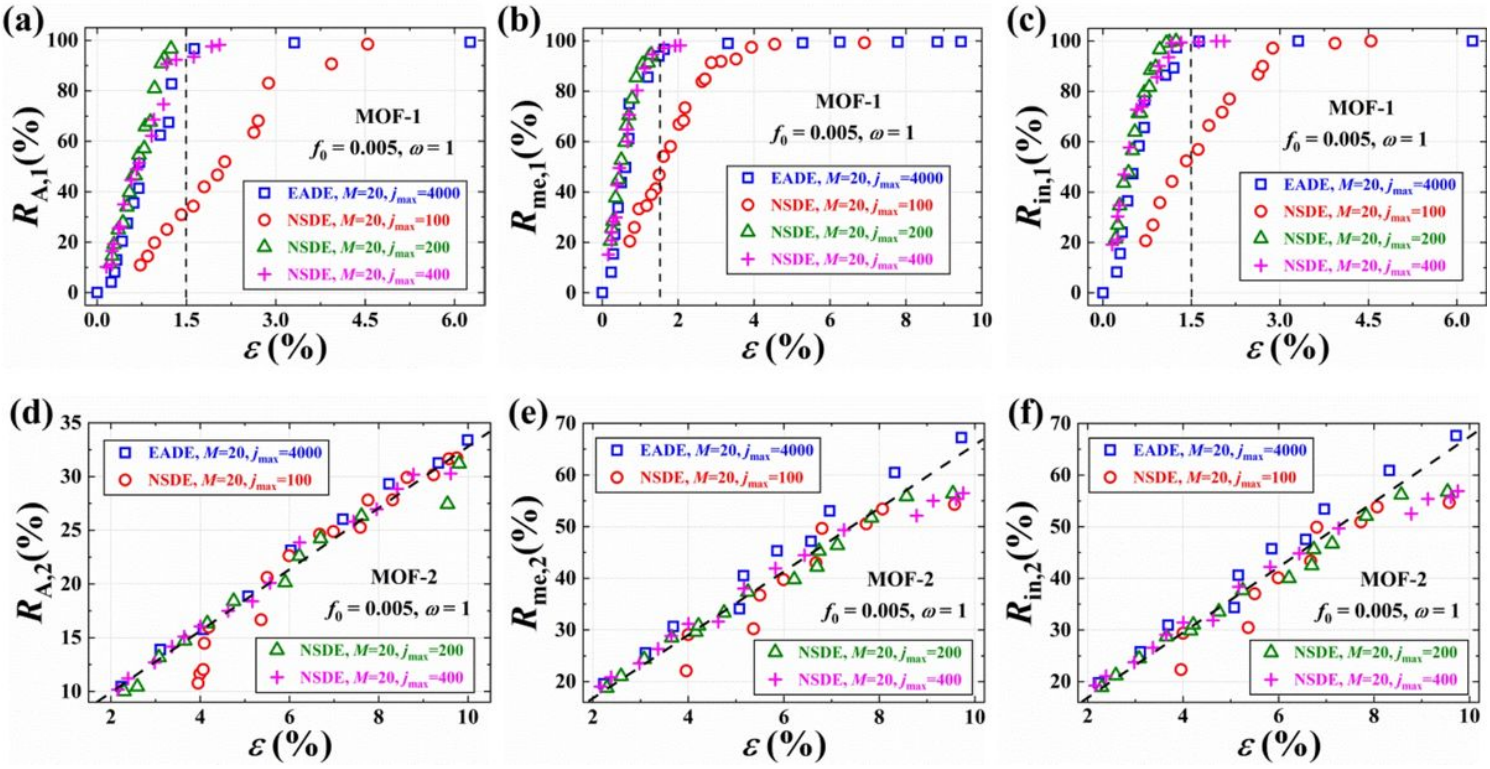

Figure 15

Pareto fronts of the LO-NES system obtained by the EADE and NSDE algorithms in single-frequency excitation condition (f0=0.005, ω=1): (a) the ε-RA,1 plane in the MOF-1; (b) the ε-Rme,1 plane in the MOF-1; (c) the ε-Rin,1 plane in the MOF-1; (d) the ε-RA,2 plane in the MOF-2; (e) the ε-Rme,2 plane in the MOF-2; (f) the ε-Rin,2 plane in the MOF-2.

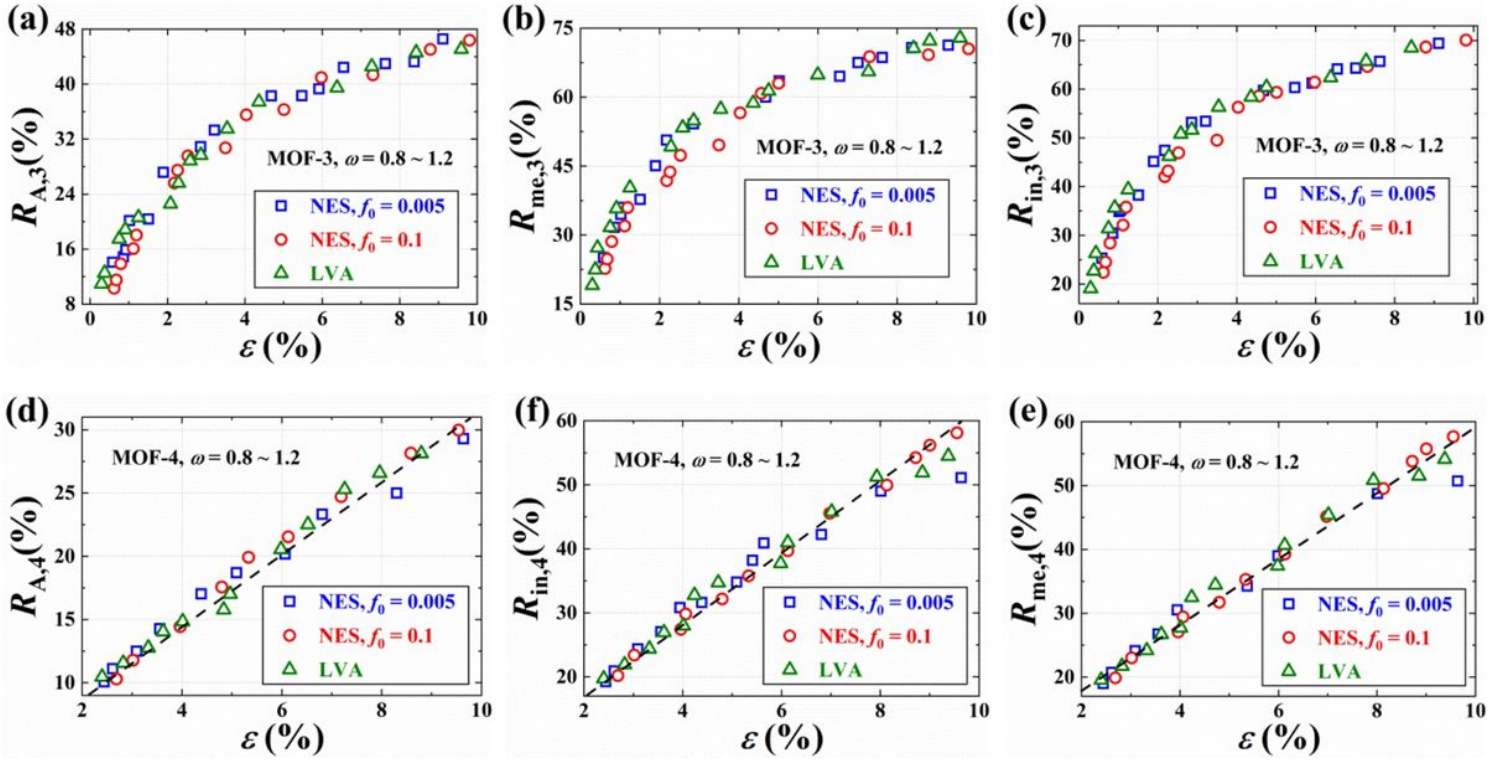

Figure 16

Pareto fronts of the LO-LVA and LO-NES systems obtained by the NSDE algorithm in sweep-frequency excitation condition (f0=0.005 or 0.1, ω=0.8~1.2): (a) the ε-RA,3 plane in the MOF-3; (b) the ε-Rme,3 plane in the MOF-3; (c) the ε-Rin,3 plane in the MOF-3; (d) the ε-RA,4 plane in the MOF-4; (e) the ε-Rme,4 plane in the MOF-4; (f) the ε-Rin,4 plane in the MOF-4.

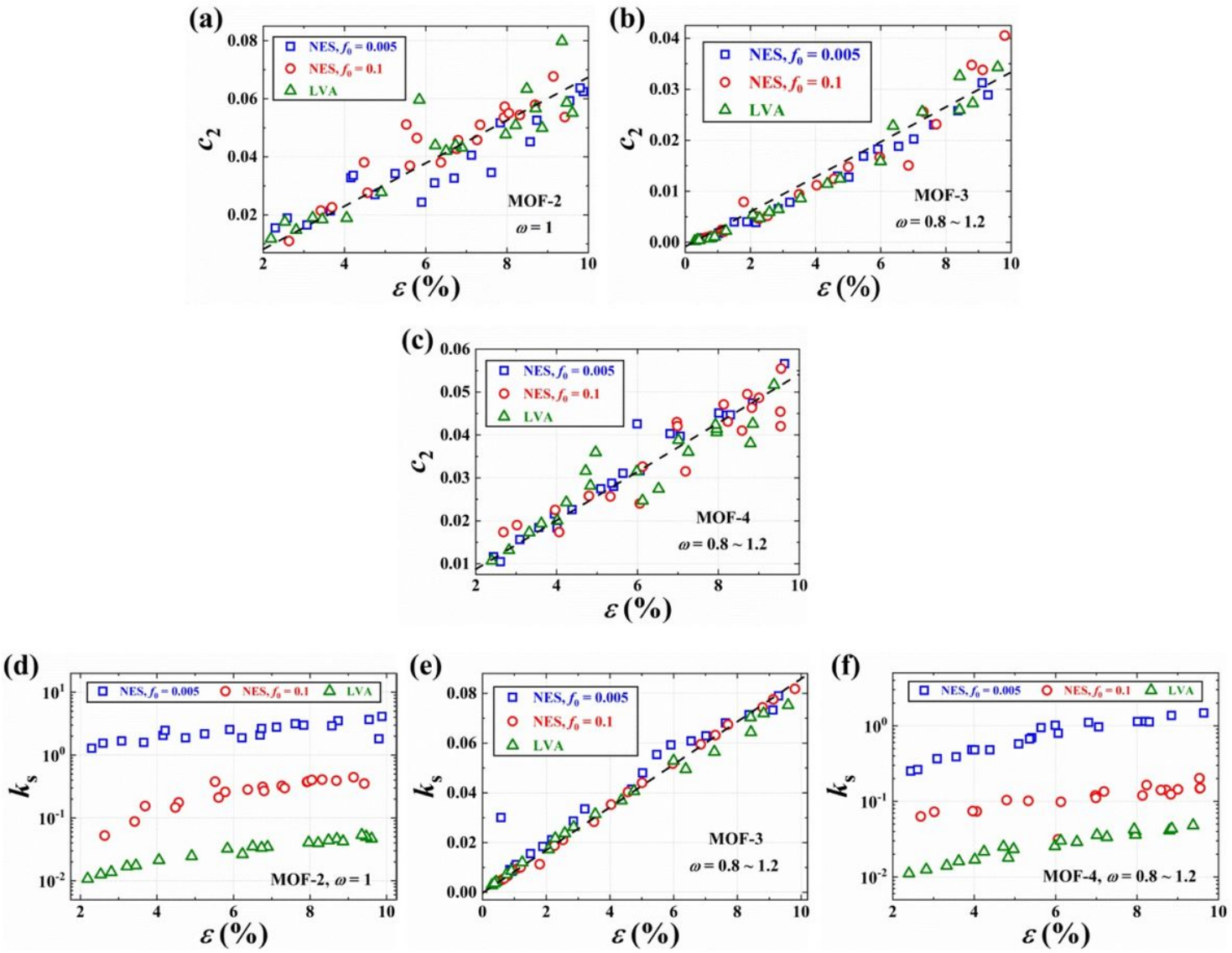

Figure 17

Trends of the optimized damping c2 and the optimized spring stiffness ks changing with the mass ratio ε obtained by the NSDE algorithm in different MOFs and excitation conditions (f0=0.005 or 0.1): (a) and (d) MOF-2; (b) and (e) MOF-3; (c) and (f) MOF-4.